nature

https://doi.org/10.1038/s41586-021-03312-w

Accelerated Article Preview

SARS-CoV-2 infection is effectively treated and prevented by EIDD-2801

Received: 18 September 2020

Accepted: 29 January 2021

Accelerated Article Preview Published online 9 February 2021

Cite this article as: Wahl, A. et al. SARS-CoV-2 infection is effectively treated and prevented by EIDD-2801. *Nature* https://doi.org/10.1038/s41586-021-03312-w (2021).

Angela Wahl, Lisa E. Gralinski, Claire E. Johnson, Wenbo Yao, Martina Kovarova, Kenneth H. Dinnon III, Hongwei Liu, Victoria J. Madden, Halina M. Krzystek, Chandrav De, Kristen K. White, Kendra Gully, Alexandra Schäfer, Tanzila Zaman, Sarah R. Leist, Paul O. Grant, Gregory R. Bluemling, Alexander A. Kolykhalov, Michael G. Natchus, Frederic B. Askin, George Painter, Edward P. Browne, Corbin D. Jones, Raymond J. Pickles, Ralph S. Baric & J. Victor Garcia

Article

SARS-CoV-2 infection is effectively treated and prevented by EIDD-2801

https://doi.org/10.1038/s41586-021-03312-w

Received: 18 September 2020

Accepted: 29 January 2021

Published online: 9 February 2021

Angela Wahl[1,2,3,16], Lisa E. Gralinski[4,16], Claire E. Johnson[1,2,3], Wenbo Yao[1,2,3], Martina Kovarova[1,2,3], Kenneth H. Dinnon III[4,5], Hongwei Liu[6,7], Victoria J. Madden[8], Halina M. Krzystek[6,7], Chandrav De[1,2,3], Kristen K. White[8], Kendra Gully[4], Alexandra Schäfer[4], Tanzila Zaman[6,7], Sarah R. Leist[4], Paul O. Grant[6,7], Gregory R. Bluemling[9,10], Alexander A. Kolykhalov[9,10], Michael G. Natchus[10], Frederic B. Askin[11], George Painter[9,10,12], Edward P. Browne[2,3,5,13], Corbin D. Jones[6,7], Raymond J. Pickles[5,14], Ralph S. Baric[4,5,15] & J. Victor Garcia[1,2,3] ✉

All known recently emerged human coronaviruses probably originated in bats[1]. Here we used a single experimental platform based on human lung-only mice (LoM) to demonstrate efficient in vivo replication of all recently emerged human coronaviruses (SARS-CoV, MERS-CoV and SARS-CoV-2) and two highly relevant endogenous pre-pandemic SARS-like bat coronaviruses. Virus replication in this model occurs in bona fide human lung tissue and does not require any type of adaptation of the virus or the host. Our results indicate that bats harbour endogenous coronaviruses capable of direct transmission into humans. Further detailed analysis of pandemic SARS-CoV-2 in vivo infection of LoM human lung tissue showed predominant infection of human lung epithelial cells, including type II pneumocytes present in alveoli and ciliated airway cells. Acute SARS-CoV-2 infection was highly cytopathic and induced a robust and sustained type I interferon and inflammatory cytokine/chemokine response. Finally, we evaluated a therapeutic and pre-exposure prophylaxis strategy for coronavirus infection. Our results show that therapeutic and prophylactic administration of EIDD-2801, an oral broad spectrum antiviral currently in phase II–III clinical trials, dramatically inhibited SARS-CoV-2 replication in vivo and thus has significant potential for the prevention and treatment of COVID-19.

The recently emerged human pandemic coronavirus Severe Acute Respiratory Syndrome coronavirus-2 (SARS-CoV-2), the causative agent of coronavirus disease (COVID)-19, has resulted in substantial morbidity and mortality worldwide[2]. Bats are the presumed source of SARS-CoV-2 and the highly pathogenic human coronaviruses SARS-CoV and Middle East Respiratory Syndrome (MERS)-CoV[1]. Transmission of coronaviruses from bats to other species is well-documented and adaptation in an intermediary host can facilitate their transmission to humans[1]. While it is possible that SARS-CoV-2 was transmitted to humans via an intermediate host, phylogenic analysis indicates that the SARS-CoV-2 lineage has circulated in bats for decades and evolved in bats into a virus capable of replicating in human cells[3]. Given the repeated and accelerating emergence of highly pathogenic coronaviruses, it is increasingly important to monitor and characterize bat coronaviruses and to identify the viral determinants of human infection, disease, and global spread as well as to develop effective therapeutic interventions. Animal models are useful in studying highly pathogenic human coronaviruses, the emergence potential of zoonotic coronaviruses, and to evaluate the *in vivo* inhibitory activity of novel agents[4–15]. However, human coronaviruses do not replicate in mice without either extensive virus adaptation, genetic editing of the host receptor, or introduction of the appropriate human receptor genes into the host[4,6–13,15]. Although existing rodent models of coronavirus infection have made several important contributions, none possesses the diverse set of primary human lung cells that serve as targets for viral infection[16]. Here, we show that human lung-only mice (LoM), immune deficient mice implanted with authentic human lung tissue[17], allow for the *in vivo* study of SARS-CoV, MERS-CoV, and SARS-CoV-2 in a single platform permitting direct comparison of experimental outcomes. Using LoM, we also show efficient replication of bat coronaviruses *in vivo* without the need for virus adaptation.

[1]International Center for the Advancement of Translational Science, University of North Carolina at Chapel Hill, Chapel Hill, NC, USA. [2]Division of Infectious Diseases, Department of Medicine, University of North Carolina at Chapel Hill, Chapel Hill, NC, USA. [3]Center for AIDS Research, University of North Carolina at Chapel Hill, Chapel Hill, NC, USA. [4]Department of Epidemiology, University of North Carolina at Chapel Hill, Chapel Hill, NC, USA. [5]Department of Microbiology and Immunology, University of North Carolina at Chapel Hill, Chapel Hill, NC, USA. [6]Department of Biology, University of North Carolina at Chapel Hill, Chapel Hill, NC, USA. [7]Department of Genetics, University of North Carolina at Chapel Hill, Chapel Hill, NC, USA. [8]Microscopy Services Laboratory, University of North Carolina at Chapel Hill, Chapel Hill, NC, USA. [9]Emory Institute of Drug Development (EIDD), Emory University, Atlanta, GA, USA. [10]Drug Innovation Ventures at Emory (DRIVE), Atlanta, GA, USA. [11]Department of Pathology, University of North Carolina at Chapel Hill, Chapel Hill, NC, USA. [12]Department of Pharmacology and Chemical Biology, Emory University, Atlanta, GA, USA. [13]UNC HIV Cure Center, University of North Carolina at Chapel Hill, Chapel Hill, NC, USA. [14]Marsico Lung Institute, University of North Carolina, Chapel Hill, NC, USA. [15]Rapidly Emerging Antiviral Drug Discovery Initiative, University of North Carolina, Chapel Hill, NC, USA. [16]These authors contributed equally: Angela Wahl, Lisa E. Gralinski. ✉e-mail: victor_garcia@med.unc.edu

In addition, we performed an in-depth *in vivo* analysis of acute SARS-CoV-2 infection in the human lung which revealed robust virus replication, pathogenesis, and sustained activation of the innate host immune response. Finally, we used this platform to show that EIDD-2801, an orally administered broad spectrum antiviral currently in phase II-III clinical trials for COVID-19 treatment, efficiently inhibited SARS-CoV-2 replication in human lung tissue when administered therapeutically and prevented SARS-CoV-2 infection when administered as pre-exposure prophylaxis strongly supporting its further clinical development for COVID-19.

Coronavirus replication in LoM

LoM are constructed by subcutaneous implantation of human lung tissue into the back of immune deficient mice (Fig. 1a). This tissue expands to form a palpable implant[17] (Fig. 1a). Lung implants contain human fibroblast, epithelial, endothelial, and mesenchymal cells that form cartilaginous and non-cartilaginous bronchial airways lined with ciliated and non-ciliated epithelium, alveolar sac structures, and extensive vasculature[17](Extended Data Fig. 1a,b). The human lung tissue in LoM has been shown to support replication of a diverse set of emerging and clinically relevant human pathogens including MERS-CoV[17].

We evaluated the potential of LoM to serve as a single platform to study all known recently emerged human coronaviruses and the potential of endogenous bat coronaviruses for human emergence. Human angiotensin converting enzyme-2 (ACE2), the receptor for SARS-CoV and SARS-CoV-2[18–21], is expressed on human epithelial cells (cytokeratin 19+) in the human lung tissues of LoM (Extended Data Fig. 1c,d). Expression of transmembrane protease serine 2 (TMPRSS2), which primes the spike protein of SARS-CoV and SARS-CoV-2[18], was also confirmed (Extended Data Fig. 1e). LoM were inoculated with SARS-CoV, MERS-CoV, or SARS-CoV-2 (Extended Data Table 1). SARS-CoV and SARS-CoV-2 infection resulted in mean virus titers of $1.76x10^8$ and $2.42x10^7$ PFU/g respectively at 2 days post-infection (Fig. 1b). Viral nucleoprotein antigen was abundantly observed in the human lung tissues of SARS-CoV and SARS-CoV-2 infected LoM (Extended Data Fig. 2a). Consistent with our previous results[17], MERS-CoV replicated to mean titers of $4.79x10^8$ PFU/g in LoM human lung tissues at 2 days post-infection (Fig. 1b) and abundant viral antigen was observed (Extended Data Fig. 2a).

Pre-pandemic bat coronaviruses WIV1-CoV and SHC014-CoV have high sequence homology to SARS-CoV, use ACE2 to infect human cells, and grow modestly in primary human airway cultures on liquid interface[12,13]. WIV1-CoV and SHC014-CoV efficiently replicated in the human lung tissue of LoM (Extended Data Table 1) with mean titers of $1.58x10^7$ and $1.48x10^7$ PFU/g, respectively at two days post-exposure (Fig. 1b) and viral antigen was readily detected in human lung tissues (Extended Data Fig. 2b). No viral antigen was detected in human lung tissues of naïve LoM (Extended Data Fig. 2c). Collectively, these results demonstrate that LoM serve as single platform where recently emerged human coronaviruses SARS-CoV, MERS-CoV, and SARS-CoV-2 replicate efficiently in human lung tissue. Importantly, the efficient replication of SARS-like bat coronaviruses WIV1-CoV and SHC014-CoV observed is in agreement with previous *in vitro* data[12,13] suggesting that bats harbor coronaviruses capable of direct transmission to humans, bypassing the need for further adaptation in an intermediary host.

SARS-CoV-2 replication in LoM

Human lung tissues of LoM were inoculated with SARS-CoV-2 and titers of replication competent virus determined 2, 6, and 14 days post-exposure (Fig. 1c, Extended Data Table 2). High titers of replication competent virus were noted at all time points although they were highest 2 days post-infection (Fig. 1c). Infection was widely distributed throughout the tissue with large numbers of cells positive for viral RNA (Fig. 1d) and nucleoprotein (Fig. 1e). Co-staining for human cytokeratin 19 demonstrated that SARS-CoV-2 predominantly infects human epithelial cells in the lung (Fig. 1f, Extended Data Fig. 3a). Viral antigen was not detected in human CD34 expressing (endothelial) cells and in only a few human vimentin expressing (mesenchymal) cells (Fig. 1f, Extended Data Fig. 3a). We further identified the types of infected epithelial cells. Virus antigen was clearly identified in cells which expressed pro-SP-C (alveolar type II [AT2] pneumocytes) or acetylated alpha-tubulin IV (ciliated cells); virus antigen was not detected in HT1-56 (alveolar type I [AT1] pneumocytes) or CC10 positive cells (club cells) (Fig. 1g, Extended Data Fig. 3b). These results demonstrate that SARS-CoV-2 has limited tropism in the lung with AT2 pneumocytes and ciliated airway epithelial cells being the predominant cells infected.

SARS-CoV-2 pathogenesis in LoM

Histopathologic analysis revealed several features of early diffuse alveolar damage that have been described in lung tissues of COVID-19 patients including the accumulation of proteinaceous exudate and fibrin in alveolar spaces, desquamation of pneumocytes, multi-nucleated cell formation, and the appearance of fibrin thrombi in small vessels (Fig. 2)[22–24]. Proteinaceous exudate, including large protein globules, was observed in alveolar spaces, which overlapped with areas of virus accumulation (Fig. 2a,b). As early as 2 days post-infection, desquamation of pneumocytes was noted; a large number of virally infected cells were fully detached or detaching from the alveolar basement membrane (Fig. 2c,d). Infected multi-nucleated cells were also observed (Fig. 2c). While hyaline membranes were not noted, in contrast to naïve LoM (Fig. 2e), fibrin was detected in alveolar spaces (Fig. 2f). Importantly, we observed multiple occluded vessels containing fibrin thrombi as reported in COVID-19 patient lungs (Fig. 2g)[22–24]. Electron microscopy demonstrated the normal architecture and integrity of uninfected AT2 pneumocytes in human lung tissue obtained from LoM two days post-infection (Fig. 2h). In contrast, AT2 cells containing virus particles in the same sample had swollen mitochondria with loss of matrix and cristae as well as rough endoplasmic reticula (RER) with distended cisternae, protein accumulation, and virus particles (Fig. 2i). Degenerative SARS-CoV-2 infected AT2 cells detached from the alveolar basal membrane were observed in the alveolar luminal space (Fig. 2j). Higher magnification revealed subcellular accumulation of virus containing vesicles indicative of virus replication and egress. Virions with electron dense nucleocapsids and distinctive crown-like spikes were observed (Fig. 2i,j). Consistent with previous reports[23,25], virions produced by human lung cells were pleomorphic in size (69 to 112 nm) and shape. Despite the extensive damage observed in the lung tissue, the endothelium in the majority of blood vessels was intact with tight junctions, numerous pinocytotic vesicles, and normal mitochondria and endoplasmic reticulum (Fig. 2k,l). Virions were not detected within endothelial cells in agreement with our immunofluorescence analysis (Fig. 1f and Fig. 2k,l). However, pleomorphic virions were present in capillary lumen surrounded by fibrillar protein deposits and cell debris (Fig. 2k,l). Together, these results demonstrate that acute SARS-CoV-2 infection of LoM closely resembles lung infection in humans and is highly cytopathic resulting in significant injury to the fragile alveolar lung structures.

We performed RNA-sequencing analysis of human lung tissues collected from animals 2, 6 and 14 days post-infection. Abundant viral transcripts were detected, ranging from 0.55% to 3.6% of the total reads at 2 days post-infection (Extended Data Table 3). Viral transcripts were abundant but lower at 6 days and 14 days post-infection (Extended Data Table 3). Sequencing data identified canonical SARS-CoV-2 transcripts[26] and confirmed maintenance of the furin cleavage site in the spike protein. Analysis of human gene transcripts revealed 1,504 differentially expressed cellular genes between naïve and infected human lung tissue at 2 days post-exposure, the peak of infection (Fig. 3a,

Supplementary Tables 1 and 2). Of these genes, differential expression analysis suggested 1,043 were increased and 461 were decreased in expression in the infected human lung tissue relative to naïve controls (Supplementary Tables 1 and 2). Three patterns of note: the expression of most genes did not change with infection, many genes with increased expression in SARS-CoV-2 infected LoM were lowly or moderately expressed in naïve LoM, and a handful of genes went from either undetectable expression in naïve LoM to moderate/high expression in infected LoM or from expression in naïve LoM to undetectable expression in infected LoM. As expected, *ACE2* and *TMPRSS2* were expressed across the lung tissues (Extended Data Table 4). Notably, numerous interferon-stimulated genes (ISGs) and inflammatory cytokine genes, including pro-inflammatory cytokines genes *IL6*, *CXCL8* (IL-8), *CXCL10* (IP-10), *TNF*, and *CCL5* (RANTES) were potently induced in infected lung tissue (Supplementary Tables 1 and 2). We also observed dramatic upregulation of *IFNB1*, *IFNL1*, *IFNL2*, and *IFNL3* expression (>1,000 fold for all) at 2 days post-exposure, suggesting that these cytokines play a key role in the antiviral response to SARS-CoV-2 (Supplementary Tables 1 and 2). Gene set enrichment analysis (GSEA) showed over 840 gene pathways significantly upregulated ($p<0.05$) including response to type 1 interferon ($p=0.0011$), response to virus ($p=0.0010$), innate immune response ($p=0.0010$), cytokine mediated signaling ($p=0.0010$), cytokine production ($p=0.0010$), response to stress ($p=0.0010$), inflammatory response, ($p=0.0010$), NIK NF-KB signaling ($p=0.0011$), acute inflammatory response ($p=0.0035$), regulation of cell death ($p=0.0030$), and coagulation pathways ($p=0.0453$) (Fig. 3b). Complement activation, which contributes to SARS-CoV pathogenesis in mouse models[14], was also increased ($p=0.0470$) (Fig. 3b). Importantly, analysis of host gene expression at later time points demonstrated a sustained upregulation of antiviral and inflammatory genes that in some instances (e.g. *ISG15*, *IFITM1*, *TNF*, *CXCL9*) persisted for up to 14 days post-infection (last time analyzed) (Fig. 3c,d, Extended Data Table 5, Supplementary Tables 1 and 2). These results demonstrate that acute SARS-CoV-2 infection causes a potent and sustained upregulation of innate immune responses in virus-infected human lung tissue.

EIDD-2801 treatment and prophylaxis

The ribonucleoside analog β-D-N^4-hydroxycytidine (NHC) broadly inhibits coronavirus infection *in vitro* in human airway epithelial cell cultures[15]. Prophylactic and therapeutic administration of its oral pro-drug EIDD-2801 (also known as molnupiravir or MK-4482) reduced SARS-CoV and MERS-CoV replication and pathogenesis in mice[15]. 5′-triphosphate NHC acts as a competitive alternate substrate for the viral RNA-dependent RNA polymerase allowing it's incorporation into viral RNA resulting in the accumulation of mutations within the viral RNA genome leading to error catastrophe[15]. As an orally bioavailable agent, EIDD-2801 could be much more readily administered to patients compared to remdesivir and other antivirals and biologics (e.g. convalescent plasma and monoclonal antibodies) which require administration by infusion in a clinical setting. We tested the ability of therapeutic EIDD-2801 to inhibit SARS-CoV-2 replication *in vivo* using a dose which is also similar to the human dose in clinical trials[27]. LoM were administered EIDD-2801 starting 24 h or 48 h post SARS-CoV-2 exposure and every 12 h thereafter (Extended Data Fig. 4a, Extended Data Table 6). Our results show that EIDD-2801 had a remarkable effect on virus replication after only two days of treatment (Fig. 4a,b). EIDD-2801 dramatically reduced the number of infectious particles in human lung tissue by 4.4 logs (>25,000 fold decrease) when treatment was initiated 24 h post-exposure ($p=0.0002$) (Fig. 4a). When treatment was started 48 h post-exposure, virus titers were significantly reduced by 96% (1.5 logs, $p=0.0019$) (Fig. 4b). Next, we tested the efficacy of EIDD-2801 pre-exposure prophylaxis. LoM were administered EIDD-2801 starting 12 h prior to SARS-CoV-2 exposure and every 12 h thereafter (Extended Data Fig. 4b, Extended Data Table 6). EIDD-2801 pre-exposure prophylaxis significantly reduced virus titers in the human lung tissues of LoM by over 100,000 fold in two independent experiments ($p=0.0002$ and $p=0.0068$, Fig. 4c–e). Furthermore, in contrast to EIDD-2801 treated mice, abundant cell debris and nucleoprotein positive cells could be readily observed in the alveolar lumen of vehicle control treated mice consistent with the extensive pathogenic effects inflicted on the lung by SARS-CoV-2 (Fig. 4f, g). These results demonstrate that prophylactic administration EIDD-2801 is highly effective at preventing SARS-CoV-2 infection and pathogenesis *in vivo*.

Discussion

Our results demonstrate replication of all known recently emerged human coronaviruses in LoM. Importantly, in agreement with *in vitro* studies[12,13], our results demonstrate relatively efficient replication of two pre-pandemic endogenous bat viruses in human lung tissue *in vivo* indicating that coronaviruses circulating in bats have pandemic potential without the need for further adaptation to humans. Acute SARS-CoV-2 infection of LoM resulted in significant lung injury and exhibited key features of the extensive lung pathology observed in severe COVID-19 patients[22,24,28,29]. In agreement with analyses of bronchoalveolar fluid obtained from COVID-19 patients and post-mortem patient lung samples[5,30], multiple ISGs were significantly increased in SARS-CoV-2 infected human lung tissue of LoM. We observed robust induction of *IFNB1* expression during acute infection followed by a decline in expression. Interestingly, an analysis of post-mortem COVID-19 patient lungs[5] did not reveal increased *IFNB1* expression and it has been shown *in vitro* that its expression is blocked during SARS-CoV infection[31,32]. These results suggest that in human lung tissue *IFNB1* expression is induced during acute SARS-CoV-2 infection. While this study was not designed to evaluate the effect of type I IFN on SARS-CoV-2 replication *in vivo*, *in vitro* studies and *in vivo* mouse studies showed that type I IFN treatment restricts SARS-CoV-2 replication[7,33]. We also observed increased expression of several human cytokine genes in SARS-CoV-2 infected LoM, many of which were also increased in analyses of COVID-19 patient serum and post-mortem lung tissue further establishing the similarities between LoM and human SARS-CoV-2 infection[5,34].

Currently, the FDA approved SARS-CoV-2 vaccines are highly effective at preventing disease. However, it may take considerable time to reach target vaccination levels needed for herd immunity, especially in resource limited settings, due to manufacturing capabilities, required vaccine shipping and storage conditions, and public acceptance. Therefore, alternative treatments and preventive approaches are still urgently needed. Remdesivir, is limited to use in hospitalized patients and its effectiveness at reducing disease and mortality late in infection is not clear[35,36]. While a carefully controlled NIH sponsored clinical trial reported that remdesivir significantly shortened the time of recovery[35], the WHO SOLIDARITY trial revealed no significant reduction in the duration of hospitalization or mortality[36]. Early administration of monoclonal antibody therapies bamlanivimab and REGN-CoV2 significantly reduced viral loads in COVID-19 patients with mild to moderate disease[37,38]. However, they must be administered by infusion in a clinical setting limiting their potential for widespread use. A highly efficacious antiviral that is administered orally has potential for more widespread use and for administration to patients with mild to moderate disease[39]. Here, we show that EIDD-2801 administered therapeutically for only two days significantly reduced infectious virus titers *in vivo* by over 4 logs. The sooner EIDD-2801 treatment was initiated after SARS-CoV-2 exposure, the greater the reduction in virus replication. We also observed that prophylactic administration of EIDD-2801 efficiently prevents SARS-CoV-2 infection *in vivo* highlighting its potential utility as an effective prophylactic and therapeutic agent against SARS-CoV-2 and other past and future zoonotic coronaviruses. NHC belongs to a class of ribonucleoside analogs known to often affect mitochondrial replication

and function. However, NHC did not cause significant mitochondrial toxicity or impair mitochondrial function *in vitro*[40]. Furthermore, no significant increase in transition frequencies in nuclear or mitochondrial message was detected in the lung tissue of ferrets dosed with EIDD-2801 for seven days consistent with the observed good tolerability of the drug[41]. Phase II and Phase II-III clinical trials are ongoing to evaluate EIDD-2801 safety and its effect on viral shedding using doses up to 1,600 mg/day twice daily, a dose that is expected to provide similar intracellular 5'-triphosphate NHC levels as a 300-500 mg/kg dose in mice. As with any antiviral, its therapeutic/prophylactic use will be dictated by risk/benefit. Limitations of our study include the absence of human nasal airway structures in LoM which are thought to be early sites of SARS-CoV-2 replication in humans[42]. Since LoM do not have an autologous human adaptive immune system they reflect the direct effect of viruses on their targets and bystander cells as well as their innate immune response to infection. Collectively, our results demonstrate the utility of LoM as a single *in vivo* platform to evaluate and compare the replication and pathogenesis of past, present, and future pre-emergent, epidemic, and pandemic coronaviruses accelerating the development and testing of therapeutic and pre-exposure prophylaxis agents such as EIDD-2801.

Online content

Any methods, additional references, Nature Research reporting summaries, source data, extended data, supplementary information, acknowledgements, peer review information; details of author contributions and competing interests; and statements of data and code availability are available at https://doi.org/10.1038/s41586-021-03312-w.

1. Cui, J., Li, F. & Shi, Z. L. Origin and evolution of pathogenic coronaviruses. *Nat Rev Microbiol* **17**, 181-192, https://doi.org/10.1038/s41579-018-0118-9 (2019).
2. Dong, E., Du, H. & Gardner, L. An interactive web-based dashboard to track COVID-19 in real time. *Lancet Infect Dis* **20**, 533-534, https://doi.org/10.1016/S1473-3099(20)30120-1 (2020).
3. Boni, M. F. *et al*. Evolutionary origins of the SARS-CoV-2 sarbecovirus lineage responsible for the COVID-19 pandemic. *Nat Microbiol*, https://doi.org/10.1038/s41564-020-0771-4 (2020).
4. Bao, L. *et al*. The pathogenicity of SARS-CoV-2 in hACE2 transgenic mice. *Nature*, https://doi.org/10.1038/s41586-020-2312-y (2020).
5. Blanco-Melo, D. *et al*. Imbalanced Host Response to SARS-CoV-2 Drives Development of COVID-19. *Cell* **181**, 1036-1045 e1039, https://doi.org/10.1016/j.cell.2020.04.026 (2020).
6. Cockrell, A. S. *et al*. A mouse model for MERS coronavirus-induced acute respiratory distress syndrome. *Nat Microbiol* **2**, 16226, https://doi.org/10.1038/nmicrobiol.2016.226 (2016).
7. Dinnon, K. H., 3rd *et al*. A mouse-adapted model of SARS-CoV-2 to test COVID-19 countermeasures. *Nature* **586**, 560-566, https://doi.org/10.1038/s41586-020-2708-8 (2020).
8. Gralinski, L. E. *et al*. Complement Activation Contributes to Severe Acute Respiratory Syndrome Coronavirus Pathogenesis. *mBio* **9**, https://doi.org/10.1128/mBio.01753-18 (2018).
9. Jiang, R. D. *et al*. Pathogenesis of SARS-CoV-2 in Transgenic Mice Expressing Human Angiotensin-Converting Enzyme 2. *Cell*, https://doi.org/10.1016/j.cell.2020.05.027 (2020).
10. McCray, P. B., Jr. *et al*. Lethal infection of K18-hACE2 mice infected with severe acute respiratory syndrome coronavirus. *J Virol* **81**, 813-821, https://doi.org/10.1128/JVI.02012-06 (2007).
11. Menachery, V. D. *et al*. Middle East Respiratory Syndrome Coronavirus Nonstructural Protein 16 Is Necessary for Interferon Resistance and Viral Pathogenesis. *mSphere* **2**, https://doi.org/10.1128/mSphere.00346-17 (2017).
12. Menachery, V. D. *et al*. A SARS-like cluster of circulating bat coronaviruses shows potential for human emergence. *Nat Med* **21**, 1508-1513, https://doi.org/10.1038/nm.3985 (2015).
13. Menachery, V. D. *et al*. SARS-like WIV1-CoV poised for human emergence. *Proc Natl Acad Sci U S A* **113**, 3048-3053, https://doi.org/10.1073/pnas.1517719113 (2016).
14. Rockx, B. *et al*. Comparative pathogenesis of COVID-19, MERS, and SARS in a nonhuman primate model. *Science* **368**, 1012-1015, https://doi.org/10.1126/science.abb7314 (2020).
15. Sheahan, T. P. *et al*. An orally bioavailable broad-spectrum antiviral inhibits SARS-CoV-2 in human airway epithelial cell cultures and multiple coronaviruses in mice. *Sci Transl Med* **12**, https://doi.org/10.1126/scitranslmed.abb5883 (2020).
16. Franks, T. J. *et al*. Resident cellular components of the human lung: current knowledge and goals for research on cell phenotyping and function. *Proc Am Thorac Soc* **5**, 763-766, https://doi.org/10.1513/pats.200803-025HR (2008).
17. Wahl, A. *et al*. Precision mouse models with expanded tropism for human pathogens. *Nat Biotechnol* **37**, 1163-1173, https://doi.org/10.1038/s41587-019-0225-9 (2019).
18. Hoffmann, M. *et al*. SARS-CoV-2 Cell Entry Depends on ACE2 and TMPRSS2 and Is Blocked by a Clinically Proven Protease Inhibitor. *Cell* **181**, 271-280 e278, https://doi.org/10.1016/j.cell.2020.02.052 (2020).
19. Li, W. *et al*. Angiotensin-converting enzyme 2 is a functional receptor for the SARS coronavirus. *Nature* **426**, 450-454, https://doi.org/10.1038/nature02145 (2003).
20. Walls, A. C. *et al*. Structure, Function, and Antigenicity of the SARS-CoV-2 Spike Glycoprotein. *Cell* **181**, 281-292 e286, https://doi.org/10.1016/j.cell.2020.02.058 (2020).
21. Yan, R. *et al*. Structural basis for the recognition of SARS-CoV-2 by full-length human ACE2. *Science* **367**, 1444-1448, https://doi.org/10.1126/science.abb2762 (2020).
22. Carsana, L. *et al*. Pulmonary post-mortem findings in a series of COVID-19 cases from northern Italy: a two-centre descriptive study. *Lancet Infect Dis*, https://doi.org/10.1016/S1473-3099(20)30434-5 (2020).
23. Menter, T. *et al*. Post-mortem examination of COVID19 patients reveals diffuse alveolar damage with severe capillary congestion and variegated findings of lungs and other organs suggesting vascular dysfunction. *Histopathology*, https://doi.org/10.1111/his.14134 (2020).
24. Tian, S. *et al*. Pulmonary Pathology of Early-Phase 2019 Novel Coronavirus (COVID-19) Pneumonia in Two Patients With Lung Cancer. *J Thorac Oncol* **15**, 700-704, https://doi.org/10.1016/j.jtho.2020.02.010 (2020).
25. Zhu, N. *et al*. A Novel Coronavirus from Patients with Pneumonia in China, 2019. *N Engl J Med* **382**, 727-733, https://doi.org/10.1056/NEJMoa2001017 (2020).
26. Kim, D. *et al*. The Architecture of SARS-CoV-2 Transcriptome. *Cell* **181**, 914-921 e910, https://doi.org/10.1016/j.cell.2020.04.011 (2020).
27. *Efficacy and Safety of Molnupiravir (MK-4482) in Hospitalized Adult Participants With COVID-19 (MK-4482-001)*, https://ClinicalTrials.gov/show/NCT04575584
28. Xu, Z. *et al*. Pathological findings of COVID-19 associated with acute respiratory distress syndrome. *Lancet Respir Med* **8**, 420-422, https://doi.org/10.1016/S2213-2600(20)30076-X (2020).
29. Zhang, H. *et al*. Histopathologic Changes and SARS-CoV-2 Immunostaining in the Lung of a Patient With COVID-19. *Ann Intern Med* **172**, 629-632, https://doi.org/10.7326/M20-0533 (2020).
30. Zhou, Z. *et al*. Heightened Innate Immune Responses in the Respiratory Tract of COVID-19 Patients. *Cell Host Microbe* **27**, 883-890 e882, https://doi.org/10.1016/j.chom.2020.04.017 (2020).
31. Siu, K. L. *et al*. Severe acute respiratory syndrome coronavirus M protein inhibits type I interferon production by impeding the formation of TRAF3.TANK.TBK1/IKKepsilon complex. *J Biol Chem* **284**, 16202-16209, https://doi.org/10.1074/jbc.M109.008227 (2009).
32. Spiegel, M. *et al*. Inhibition of Beta interferon induction by severe acute respiratory syndrome coronavirus suggests a two-step model for activation of interferon regulatory factor 3. *J Virol* **79**, 2079-2086, https://doi.org/10.1128/JVI.79.4.2079-2086.2005 (2005).
33. Vanderheiden, A. *et al*. Type I and Type III Interferons Restrict SARS-CoV-2 Infection of Human Airway Epithelial Cultures. *J Virol* **94**, https://doi.org/10.1128/JVI.00985-20 (2020).
34. Qin, C. *et al*. Dysregulation of immune response in patients with COVID-19 in Wuhan, China. *Clin Infect Dis*, https://doi.org/10.1093/cid/ciaa248 (2020).
35. Beigel, J. H. *et al*. Remdesivir for the Treatment of Covid-19 - Final Report. *N Engl J Med*, https://doi.org/10.1056/NEJMoa2007764 (2020).
36. Pan, H. *et al*. Repurposed antiviral drugs for COVID-19 –interim WHO SOLIDARITY trial results. 2020.2010.2015.20209817, doi: 10.1101/2020.10.15.20209817%J medRxiv (2020).
37. Chen, P. *et al*. SARS-CoV-2 Neutralizing Antibody LY-CoV555 in Outpatients with Covid-19. https://doi.org/10.1056/NEJMoa2029849 (2020).
38. Regeneron Pharmaceuticals, I. (TARRYTOWN, N.Y., 2020).
39. Kim, P. S., Read, S. W. & Fauci, A. S. Therapy for Early COVID-19: A Critical Need. *JAMA*, https://doi.org/10.1001/jama.2020.22813 (2020).
40. Sticher, Z. M. *et al*. Analysis of the Potential for N (4)-Hydroxycytidine To Inhibit Mitochondrial Replication and Function. *Antimicrob Agents Chemother* **64**, https://doi.org/10.1128/AAC.01719-19 (2020).
41. Toots, M. *et al*. Characterization of orally efficacious influenza drug with high resistance barrier in ferrets and human airway epithelia. *Sci Transl Med* **11**, https://doi.org/10.1126/scitranslmed.aax5866 (2019).
42. Hou, Y. J. *et al*. SARS-CoV-2 Reverse Genetics Reveals a Variable Infection Gradient in the Respiratory Tract. *Cell*, https://doi.org/10.1016/j.cell.2020.05.042 (2020).

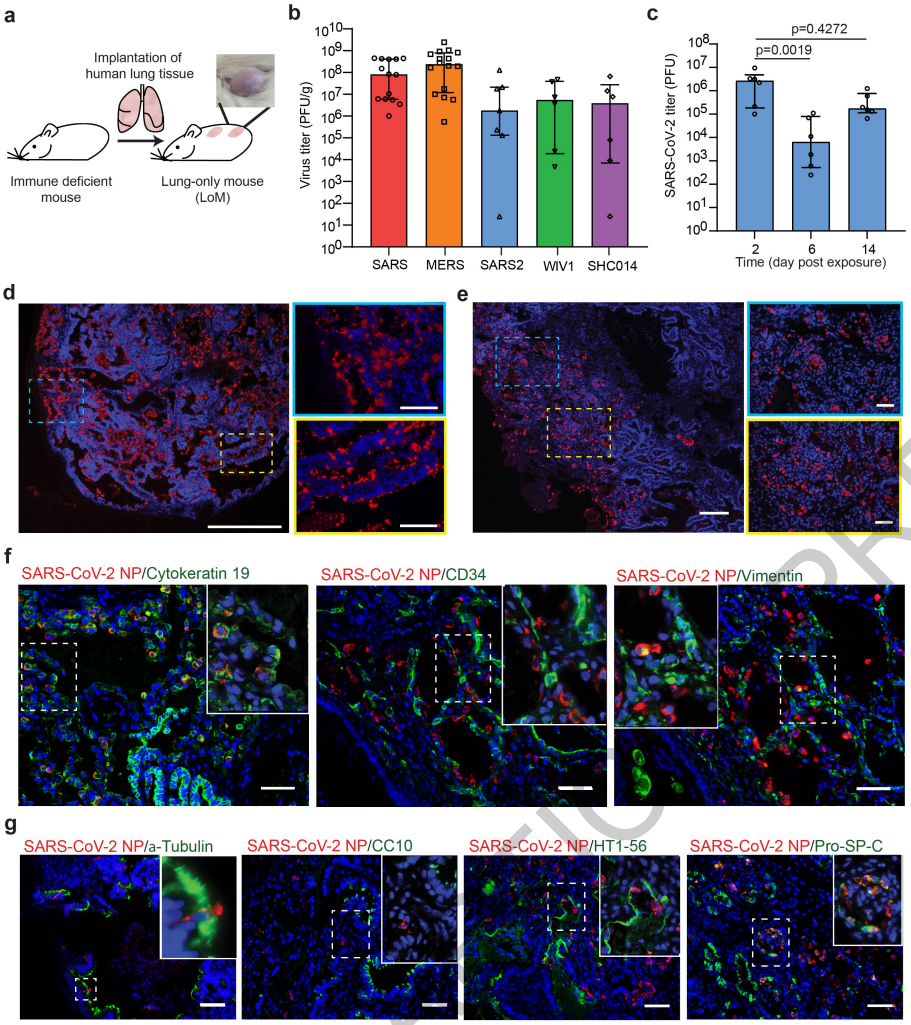

Fig. 1 | Robust replication of recently emerged human and bat coronaviruses in LoM demonstrate the potential of bat coronaviruses for direct transmission to humans and the predilection of SARS-CoV-2 for infection of human epithelial cells. a, LoM construction and image of a human lung implant. **b**, Viral titers in the human lung tissue of LoM injected with SARS-CoV (n=14, red), MERS-CoV (n=16, orange), SARS-CoV-2 (n=7, blue), WIV1-CoV (n=6, green), or SHC014 (n=6, purple) as determined by plaque assay (PFU, plaque forming units). **c**, SARS-CoV-2 titers in the human lung tissue of LoM at days 2 (n=6), 6 (n=6), and 14 (n=6) post-exposure were compared with a two-sided Kruskal-Wallis with Dunn's multiple comparisons test. **d**, SARS-CoV-2 RNA in LoM human lung tissue 2 days post-exposure (SARS-CoV-2 RNA+, red; nuclei, blue; scale bars, 750 um [left image] and 250 um [right images], n=3). **e**, Virus nucleoprotein in LoM human lung tissue two-days post-exposure (positive cells, red; nuclei, blue; scale bars 200 um [left image] and 50 um [right images], n=6). **f**, Co-staining of LoM human lung tissue two days following SARS-CoV-2 exposure for virus nucleoprotein (red) and cytokeratin 19 (epithelial cells, green, n=6), CD34 (endothelial cells, green, n= 4), or vimentin (mesenchymal cells, green, n=4). Nuclei, blue; scale bars 50 um. **g**, Co-staining of LoM human lung tissue two days following SARS-CoV-2 exposure for virus nucleoprotein (red) and acetylated alpha-tubulin IV (ciliated cells, green, n=6), CC10 (club cells, green, n=6), HT1-56 (alveolar type 1 cells, green, n=6), or Pro-SP-C (alveolar type 2 cells, green, n=3). Nuclei, blue; scale bars 50 um. In **b** and **c**, horizontal and vertical lines represent the median and interquartile range respectively. n= number of biologically independent lung tissues analyzed.

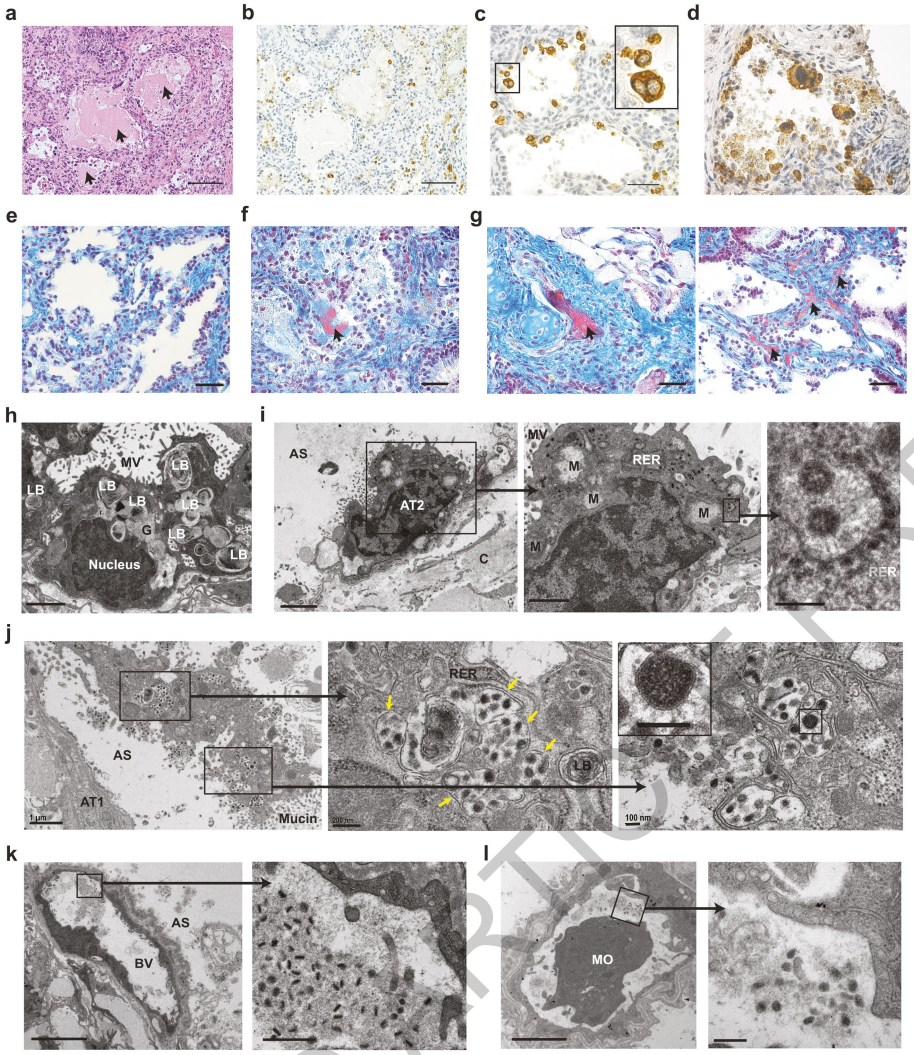

Fig. 2 | Acute SARS-CoV-2 infection is highly cytopathic and causes extensive damage to human lung structures. a, H&E staining of a SARS-CoV-2 infected LoM human lung tissue 2 days post-exposure (scale bar, 100 um, n=6). Arrows indicate protein globules. **b-d**, Immunohistochemical staining for virus nucleoprotein in LoM human lung tissue 2 days following SARS-CoV-2 exposure (positive cells, brown; **b** scale bars, 100 um; **c** and **d** scale bars, 50 um, n=6). **e-g**, Martius Scarlet Blue staining of human lung tissue from **e**, naïve LoM (n=6) and **f** and **g**, SARS-CoV-2 infected LoM 2 days post-exposure (scale bars, 50 um; fibrin, red; collagen, blue, n=6). Arrows indicate the presence of fibrin (red) in **f**, alveoli or in **g**, thrombi of occluded vessels. **h-l**, Electron microscopy analysis of SARS-CoV-2 infected human lung tissue two days post-exposure (n=3). **h**, Uninfected AT2 cells in an alveolus-like structure. Scale bars, 2 um. **i**, SARS-CoV-2 infected AT2 cell. Higher magnification images of boxed areas show virus particles with dense nucleocapsids in RER. Scale bars, 2 um (left image), 1 um (middle image), and 200 nm (right image). **j**, Degenerative SARS-CoV-2 infected cell in the alveolar space. Arrows indicate virus filled vesicles. Scale bars, 1 um (left image), 200 nm (middle image), and 100 nm (right image). **k** and **l**, Blood vessels containing virions, fibrillar protein and cell debris. In **k**, scale bars, 5 um (left image) and 500 nm (right image). In **l**, scale bars, 2 um (right image) and 200 nm (left image). AS, alveolar space; AT1, alveolar type 1 cells; AT2, alveolar type 2 cells; BV, blood vessel; C, collagen; G, glycogen; LB, lamellar body; M, mitochondria; MO, monocyte; MV, microvilli; RER, rough endoplasmic reticulum. In **c**, **i-l**, black boxes indicate areas of higher magnification images. n= number of biologically independent lung tissues analyzed.

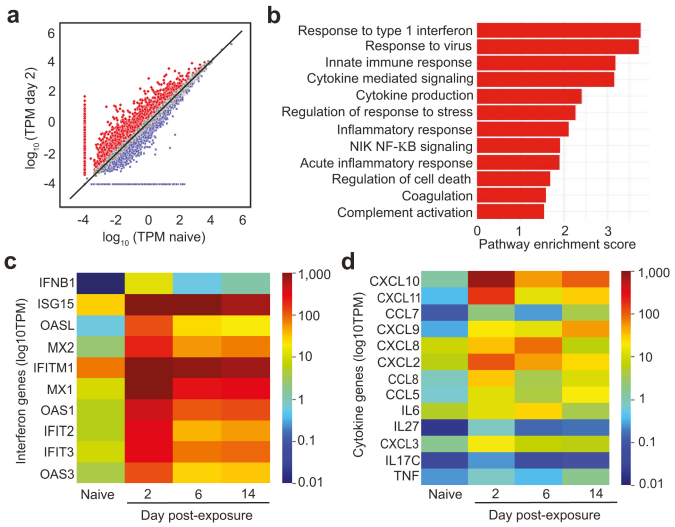

Fig. 3 | SARS-CoV-2 infection induces a strong and sustained host innate immune response in human lung tissue. a-d, RNA-sequencing analysis of human lung tissue collected from SARS-CoV-2 infected LoM. **a**, Log_{10} gene transcripts per million (TPM) in the human lungs of naïve LoM (n=2, x-axis) and SARS-CoV-2 infected (n=2, y-axis) LoM day 2 post-exposure. Genes of interest from Supplementary Tables 1 and 2 that appear increased (red) or decreased (blue) at least two-fold in SARS-CoV-2 infected LoM are shown. Genes having zero (0) mean TPM in either naïve or infected LoM are set at a minimum of log10 (0.0001) TPM in order to visualize. **b**, Gene set enrichment analysis (GSEA) identified gene sets enriched in SARS-CoV-2 infected LoM human lungs. The pathway enrichment score is shown on the x-axis. The statistical significance of enrichment scores was determined using a two-sided empirical phenotype-based permutation test and adjusted for multiple testing using a False Discovery Rate (red, $p<0.05$). Heatmaps illustrating the expression of human **c**, interferon genes and **d**, cytokine/chemokine genes in human lung tissue collected analyzed from SARS-CoV-2 infected LoM days 2 (n=2), 6 (n=3), and 14 (n=3) post-exposure and naïve LoMs (n=4). Color scale indicates the mean log_{10} TPM. n= number of biologically independent lung tissues analyzed.

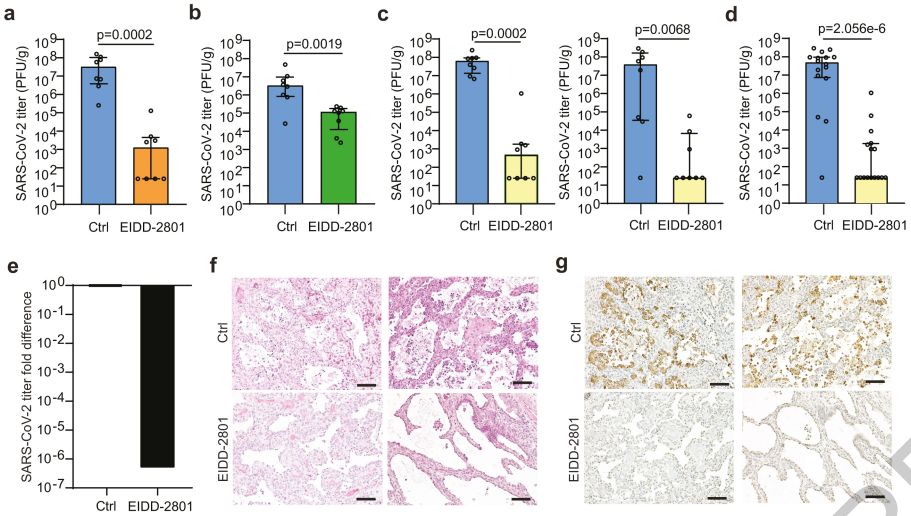

Fig. 4 | Treatment and pre-exposure prophylaxis with EIDD-2801, a broad-spectrum anti-coronavirus drug, potently inhibit SARS-CoV-2 infection *in vivo*. **a**, SARS-CoV-2 titers in the human lung tissue of LoM administered EIDD-2801 (n=8) or vehicle (n=8) 24 h post virus exposure. **b**, SARS-CoV-2 titers in the human lung tissue of LoM administered EIDD-2801 (n=8) or vehicle (n=8) 48 h post virus exposure. **c** and **d**, SARS-CoV-2 titers in the human lung tissue of LoM administered EIDD-2801 (n=8 per experiment, yellow) or control vehicle (Ctrl, n=8 per experiment, blue) at 2 days post-exposure in two independent experiments shown **c**, separately and **d**, combined. **e**, Fold difference in SARS-CoV-2 titers in the human lung tissue of LoM relative to vehicle controls. **f**, H&E staining and **g**, immunohistochemical staining for virus nucleoprotein (positive cells, brown) of human lung tissue of LoM administered EIDD-2801 (n=8) or control vehicle (Ctrl, n=8) at 2 days post-exposure (scale bars, 100 um). **a**-**d**, Titers were compared with a two-tailed Mann-Whitney U test. Horizontal and vertical lines represent the median and interquartile range respectively. n= number of biologically independent lung tissues analyzed.

Methods

Ethics statement

Animal studies were carried out according to protocols approved by the Institutional Use and Care Committee at UNC-Chapel Hill and in adherence to the NIH Guide for the Care and Use of Laboratory Animals. Mice were kept on a 12 h light/12 h dark cycle and housed in a temperature (20-23 °C) and humidity (30-70%) controlled vivarium maintained by the Division of Comparative Medicine at the University of North Carolina-Chapel Hill.

Experimental design

Human lung-only mice (LoM) were used as an *in vivo* model to evaluate infection of lung tissue with recombinant coronaviruses SARS-CoV, MERS-CoV, and SARS-CoV-2 as well as full length bat coronaviruses WIV1 and SHC014[12,13,43,44]. Viruses were directly injected into the human lung tissue of LoMs and lung tissue collected either 2, 6, or 14 days post-exposure for virus titer determination and/or analysis by histology, electron microscopy, or RNA-seq.

Construction of humanized mice

LoMs were constructed with 1-2 human lung implants by surgically implanting human lung tissue (Advanced Bioscience Resources) subcutaneously into the upper and lower back of male and female 12-21 week old NOD.Cg-Prkdc^{scid} Il2rg^{tm1Wjl}/SzJ mice [NSG mice; The Jackson Laboratory] as previously described[17]. Engraftment of lung tissue was assessed by palpation and by 8 weeks post-surgery animals were ready for experimentation.

Production of coronavirus stocks and infection of humanized mice

Stocks of wild-type SARS-CoV, MERS-CoV (HCoV-EMC/2012), SHC014-CoV, and WIV1-CoV were derived from infectious virus clones and were prepared and titered on Vero E6 (SARS-CoV, SHC014-CoV, and WIV1-CoV) or Vero CCL81 cells (MERS-CoV) (American Type Culture Collection) as previously described[6,12,13,17]. Cell lines were authenticated by morphological identification and virus susceptibility profiles and tested for mycoplasma by the supplier. A clinical isolate of SARS-CoV-2 (2019-nCoV/USA-WA1/2020) was obtained from the U.S. Centers for Disease Control and Prevention (GenBank accession no. MN985325.1) and passaged twice in Vero E6 cells to create a passage 5 working stock[42]. For the infection of mice with coronavirus, the fur over the human lung tissue of anesthetized mice was shaved and virus (1-3x10^5 PFU in 100 ul PBS) was injected directly into the lung tissue. To evaluate the *in vivo* inhibitory activity of EIDD-2801 pre-exposure prophylaxis, mice were administered 500 mg/kg EIDD-2801 or vehicle control (10% PEG and 2.5% Cremophor RH40 in water) via oral gavage starting 12 h prior to SARS-CoV-2 exposure and every 12 h thereafter. The therapeutic efficacy of EIDD-2801 was assessed by administering mice 500 mg/kg EIDD-2801 or vehicle control (10% PEG and 2.5% Cremophor RH40 in water) via oral gavage starting 24 h or 48 h post exposure and every 12 h thereafter. At necropsy, human lung tissues were collected, weighed (mean weight: 0.55 grams ± 0.05 s.e.m, n=32), homogenized, and stored at -80 °C until tittering on Vero E6 cells. Titers below the limit of the assay (50 PFU/mL) were assigned a value of 25 PFU/gram. No correlation was observed between SARS-CoV-2 titers (PFU/g) at 2 days post-exposure and the timing post-surgery (p=0.4474, two-tailed Spearman's rank correlation).

H&E staining of human lung tissue

Human lung tissues collected from LoM were fixed in 10% formalin, paraffin embedded, and cut into 5 µm sections which were mounted onto Superfrost Plus slides (Fisher Scientific). Tissue sections were incubated at 60 °C for 1 h, deparaffinized with xylene (2 × 3 min) and graded ethanol (100% 2 × 3 min, 95% 1 × 3 min, 80% 1x 3min, 70% 1 × 3 min), and stained with hematoxylin followed by eosin. Tissue sections were then mounted and imaged on a Nikon Eclipse Ci microscope using Nikon Elements BR software (version 4.30.01) with a Nikon Digital Sight DS-Fi2 camera. Brightness, contrast and white balance were adjusted on whole images in Adobe Photoshop (CS6).

Immunohistochemical analysis of coronavirus infection

Immunohistochemistry was performed as previously described[17]. Briefly, fixed (10% formalin) human lung tissues collected from coronavirus-infected LoM were paraffin embedded and sectioned (5 um). Tissue sections mounted on Superfrost Plus slides (Fisher Scientific) were deparaffinized as described above. Following antigen retrieval using Diva Decloaker (BioCare Medical), non-specific binding was blocked using Background Sniper (BioCare Medical). Tissue sections were then incubated with primary antibodies against SARS-CoV nucleocapsid (1:500 or 1:1,000), MERS-CoV nucleocapsid (1:2,000), or TMPRSS2 (1:100) overnight at 4 °C. Tissue sections incubated with rabbit IgG were used as isotype controls. Tissue sections were then washed in TBST and the endogenous peroxidase activity blocked with hydrogen peroxide. Tissue sections were developed using the MACH-3 polymer system (BioCare Medical) and 3,3′-diaminobenzidine (DAB) (Vector Laboratories), counterstained with hematoxylin, and mounted. Tissue sections were imaged on a Nikon Eclipse Ci microscope using Nikon Elements BR software (version 4.30.01) with a Nikon Digital Sight DS-Fi2 camera. Adobe Photoshop (CS6) was used to adjust brightness, contrast and white balance on whole images.

Immunofluorescence analysis of SARS-CoV2 infection

Human lung tissues collected from mice were fixed in 10% formalin and paraffin embedded. Immunofluoresence staining of 5 um tissue sections was performed as previously described[17]. Briefly, following deparaffinization and antigen retrieval (Diva Decloaker), tissue sections were incubated with a 10% normal donkey serum solution with 0.1% Triton X-100 in 1x PBS to block non-specific binding. Tissue sections were then incubated overnight with primary antibodies at 4 °C followed by incubation with fluorescent conjugated secondary antibodies. Primary antibodies were directed against SARS nucleoprotein (1:500 or 1:1,000), ACE2 (1:200), human cytokeratin 19 (1:250), CD34 (1:100), vimentin (1:100), acetylated alpha-tubulin IV, CC10 (1:500), HT1-56 (1:150), and pro-SP-C (1:500). Secondary antibodies were: Donkey anti-Mouse IgG heavy and light chains-AlexaFluor 488 (1:1,000), Donkey anti-Rabbit IgG heavy and light chains-AlexaFluor 488(1:1,000), Donkey anti-Goat IgG heavy and light chains-AlexaFluor 594 (1:1,000), Donkey anti-Mouse IgG heavy and light chains-AlexaFluor Plus 594 (1:1,000),

Donkey anti-Rabbit IgG heavy and light chains-AlexaFluor Plus 594 (1:1,000), Donkey anti-Mouse IgG heavy and light chains-AlexaFluor 647 (1:1,000). Background autofluorescence was then quenched using a 0.1% Sudan Black B solution in 80% ethanol prior to staining with DAPI. Slides were mounted and then imaged using an Olympus BX61 upright wide-field microscope using Volocity software (version 6.3) with a Hamamatsu ORCA RC camera. Appropriate negative controls without primary antibodies were also imaged using the same exposure time as matching stained sections. Whole image contrast, brightness, and pseudocoloring were adjusted using ImageJ/Fiji (Version 2.0.0-rc-69/1.51w) and Adobe Photoshop (version CS6).

RNA in situ hybridization (RNA-ISH) analysis of SARS-CoV2 infection

RNA-ISH was performed on 10% formalin fixed, paraffin-embedded, 5 µm sections of human lung tissues using the RNAscope 2.5 HD Reagent Kit according to the manufacturer's instructions (Advanced Cell Diagnostics). Briefly, tissue sections were mounted on Superfrost Plus microscope slides (Fisher Scientific), heated at 60 °C for 1 h, deparaffinized in xylene (2 x 5 minutes) and 100% ethanol (2x2 minutes),

and air-dried. Tissue sections were then incubated with hydrogen peroxide to block endogenous peroxidases for 10 min at RT, followed by epitope retrieval (Advanced Cell Diagnostics) for 30 min in a 95 °C water bath. Subsequently, tissue sections were immediately washed in double distilled water then dehydrated in 100% ethanol for 2 min before air-drying. Tissue sections were then incubated with Protease Plus (Advanced Cell Diagnostics) for 30 min at 40 °C in a HybEZ hybridization oven (Advanced Cell Diagnostics). Sections were rinsed 3 times in double distilled water and then incubated with pre-warmed target probe designed to hybridize with the spike protein of SARS-CoV-2 (Cat. Number 848561, Advanced Cell Diagnostics) for 2 h at 40 °C. Tissue sections were then washed and the signal amplified according to the manufacturer's instructions and developed using alkaline phosphatase and Fast Red substrate. Tissue sections were counterstained with DAPI, mounted with Prolong® Gold (Invitrogen), and imaged on an EVOS M5000 microscope (Invitrogen).

Electron microscopy analysis of SARS-CoV2 infection

Small pieces of human lung tissue collected from SARS-CoV-2 infected LoM at two days post-infection were fixed in 4% paraformaldehyde/2.5% glutaraldehyde in 0.15 M sodium phosphate buffer, pH 7.4, for 2 h at RT. The tissues were subsequently transferred to 10% formalin for 7 days. Specimens were washed in 0.1 M sodium cacodylate, pH 7.4, then post-fixed with 1% cacodylate-buffered osmium tetroxide for 1 h. After washing in 0.05 M sodium cacodylate buffer, pH 7.0, the samples were treated with 1% tannic acid in 0.05 M sodium cacodylate buffer for 30 min to enhance tissue contrast and preserve structure[45]. Tissue pieces were washed in deionized water, dehydrated in ethanol, and placed through two exchanges of propylene oxide before infiltration and embedment in PolyBed 812 epoxy resin (Polysciences). Semi-thin (1 µm) sections of tissue blocks were cut and stained with 1% toluidine blue in 1% sodium borate for examination by light microscopy. Ultra-thin (70 nm) sections were cut of selected regions of interest, mounted on 200 mesh copper grids and stained with 4% aqueous uranyl acetate and Reynolds' lead citrate. Grids were observed on a JEOL JEM 1230 transmission electron microscope operating at 80kV (JEOL USA, Inc.) and images were acquired with a Gatan Orius SC1000 CCD Digital Camera and Gatan Microscopy Suite software (version 3.0, Gatan, Inc.). Virus particle sizes were measured in Fiji/Image J (version 2.0.0-rc-69/1.52p).

Processing of human lung tissues for RNA-sequencing analysis

Human lung tissues were collected in RNAlater and kept at 4 °C for 24 h prior to storage at -80 °C until further processing. To isolate RNA, samples stored in RNAlater were thawed and the tissue transferred to a new tube containing 1 mm glass beads and 1 mL Trizol. Tissues were subsequently homogenized using a MagNA Lyser (Roche) for 30 sec at 6,000 rpm. In between rounds of homogenization, tissues were incubated on ice for 1 min. Following tissue homogenization, Trizol homogenate was transferred to a new tube and stored at -80 °C.

RNA-sequencing analysis

RNA was extracted from lung samples using a Trizol Plus RNA extraction kit (Thermo Fisher), quantified using a Qubit RNA assay kit and checked for quality using a Bioanalyzer RNA600 Nano kit (Agilent). RNA integrity scores were typically 7.0 and greater. 1ug of RNA was used to construct libraries for sequencing using a NEBNext Ultra II library prep kit with polyA RNA selection. Barcoded libraries were sequenced on a Novaseq 6,000 2x100 bp following manufacturer's instructions (Illumina). Sequence quality was assessed using FASTQC (version 0.11.9). No issues were detected with the data and quality was typical for RNA extracted from fresh frozen material. A small amount of index hopping was detected (0.09%) due to the single indices used in the library preparation. Raw reads were mapped to the human, mouse, and SARS-CoV-2 reference genomes simultaneously (GRCh38.p13, GRCm38.p6 M25, NC_045512, respectively) using the BBsplit function in BBmap (version 38.86). This step minimized cross mapping of reads among genomes. There was a non-significant, negative relationship between the amount of viral and human RNA reads (R2=0.136). We then mapped and quantified on a transcript and gene model basis using STAR (version 2.7.5a) and Salmon (version 1.2.1)[46,47]. Reads mapping to multiple locations were dropped from analysis. On average, in the lung tissue samples from LoM mice, 80% of the reads mapped to human (standard deviation: +/- 6%), 19% mapped to mouse (standard deviation: +/- 6%) and 1% mapped to the SARS-CoV-2 genome (standard deviation: +/- 1%). The percent of virus ranged from 0.05% to 3.4% among infected mice, with day 2 mice having the most, which is consistent with the infection titers observed. Samples from naïve mice were 95% or more human data.

Statistics and reproducibility

No statistical methods were used to predetermine sample size. No randomization was used to determine allocation of samples/animals to experimental groups and downstream analysis. The investigators were not blinded to group allocation for data collection and analysis. In Fig. 1b, titers for SARS-CoV and MERS-CoV represent two independent experiments and titers for SARS-CoV-2, WIV1-CoV, and SHC014-CoV represent one experiment. Virus titers between SARS-CoV-2 infected LoMs analyzed 2 post-exposure and days 6 and 14 post-exposure (Fig. 1c) were compared with a two-sided Kruskal-Wallis with Dunn's multiple comparisons test and data represents one experiment. Pieces of human lung implants obtained from LoM in Fig. 1c were used for the RNAscope and immunofluorescence analysis shown in Fig. 1d–g, the histological and EM analyses in Fig. 2, and the RNA-seq gene expression analyses in Fig. 3, Extended Data Fig. 3, Extended Data Tables 3-5, and Supplementary Tables 1 and 2. The number of independent LoM human lung tissue samples analyzed for each parameter is indicated in the figure and table legends. RNA-sequencing data was normalized and interrogated for changes in gene expression using DESeq2 package (version 3.1.1) in R (version 3.6.3)[48] and statistical tests were two-sided. We focused the analysis on the naïve controls versus LoM for days 2, 6, and 14 post-infection. Wald's tests were performed contrasting each day versus naïve controls. Because mice were sacrificed at each time point, we treated each day independently and not as a time series. *P*-values were adjusted for multiple testing using a False Discovery Rate using the Benjamini & Hochberg method[49]. Data was analyzed both jointly and within each treatment compared to naïve controls. Differential expression of outliers was assessed and found insignificant in overall effect. Graphs and summary tables were built in R using ggplot; gene set enrichment was performed using GSEA and GO analysis (tidyverse 1.3.0; PCATools 1.2.0; Sqldf 0.4-11; na.tools 0.3.1; ggbiplot 0.55; ggplot2 3.3.1; dplyr 0.8.4). The statistical significance of GSEA calculated enrichment scores was determined using an empirical phenotype-based permutation test[50] and *P*-values adjusted for multiple testing using a False Discovery Rate using the Benjamini & Hochberg method[49]. Specific gene sets of interest were then interrogated for patterns of expression across treatment and time using unsupervised clustering of normalized gene expression counts. Gene Ontology (GO) analysis and visualization were performed with Gorilla (no version)[51]. Data was uploaded to the NCBI GEO archive (accession: GSE155286). In Fig. 4, virus titers in vehicle control and EIDD-2801 dosed LoM were compared with a two-sided Mann-Whitney U test (GraphPad Prism, version 8.0 or R, version 3.5.3). The effect of EIDD-2801 treatment on virus titers (Fig. 4a,b) represents one experiment and the effect of EIDD-2801 prophylaxis (Fig. 4c–e) represents two independent experiments. All independent attempts of repetition were completed with similar results.

Reporting summary

Further information on research design is available in the Nature Research Reporting Summary linked to this paper.

Data availability

Gene-expression data are available at the Gene Expression Omnibus (GEO) repository (accession: GSE155286). Source data is provided for Fig. 1b, c and Fig. 4a–d. All other data is available from corresponding authors on reasonable request. Publicly available data sets used in this study: 1) sequence of the SARS-CoV-2 strain 2019-nCoV/USA-WA1/2020 (GenBank accession: MN985325.1) and 2) human lung tissue gene expression data profiled by the GTEx project (https://gtexportal.org/home/; data retrieved 10/20/2020 and 11/3/2020). Source data are provided with this paper.

43. Scobey, T. *et al*. Reverse genetics with a full-length infectious cDNA of the Middle East respiratory syndrome coronavirus. *Proc Natl Acad Sci U S A* **110**, 16157-16162, https://doi.org/10.1073/pnas.1311542110 (2013).
44. Yount, B. *et al*. Reverse genetics with a full-length infectious cDNA of severe acute respiratory syndrome coronavirus. *Proc Natl Acad Sci U S A* **100**, 12995-13000, https://doi.org/10.1073/pnas.1735582100 (2003).
45. Simionescu, N. & Simionescu, M. Galloylglucoses of low molecular weight as mordant in electron microscopy. I. Procedure, and evidence for mordanting effect. *J Cell Biol* **70**, 608-621, https://doi.org/10.1083/jcb.70.3.608 (1976).
46. Dobin, A. *et al*. STAR: ultrafast universal RNA-seq aligner. *Bioinformatics* **29**, 15-21, https://doi.org/10.1093/bioinformatics/bts635 (2013).
47. Patro, R., Duggal, G., Love, M. I., Irizarry, R. A. & Kingsford, C. Salmon provides fast and bias-aware quantification of transcript expression. *Nat Methods* **14**, 417-419, https://doi.org/10.1038/nmeth.4197 (2017).
48. Love, M. I., Huber, W. & Anders, S. Moderated estimation of fold change and dispersion for RNA-seq data with DESeq2. *Genome Biol* **15**, 550, https://doi.org/10.1186/s13059-014-0550-8 (2014).
49. Benjamini, Y. & Hochberg, Y. Controlling the False Discovery Rate: A Practical and Powerful Approach to Multiple Testing. **57**, 289-300, https://doi.org/10.1111/j.2517-6161.1995.tb02031.x (1995).
50. Subramanian, A. *et al*. Gene set enrichment analysis: a knowledge-based approach for interpreting genome-wide expression profiles. *Proc Natl Acad Sci U S A* **102**, 15545-15550, https://doi.org/10.1073/pnas.0506580102 (2005).
51. Eden, E., Navon, R., Steinfeld, I., Lipson, D. & Yakhini, Z. GOrilla: a tool for discovery and visualization of enriched GO terms in ranked gene lists. *BMC Bioinformatics* **10**, 48, https://doi.org/10.1186/1471-2105-10-48 (2009).

Acknowledgements We thank current and past members of the Garcia laboratory for technical assistance. The authors also thank technicians at the UNC Animal Histopathology and Laboratory Animal Medicine Core and Division of Comparative Medicine. We also thank the UNC School of Medicine Bioinformatics and Analytics Research Collaborative (BARC) for providing technical support and K. Mollan and B. Shook-Sa of the UNC CFAR Biostatistics Core for providing statistical support. **Funding:** This work was supported by funding from National Institutes of Health grants R21AI113736 (RJP), U19AI100625 and R01 AI108197 (RSB), Fast Grants (LEG), R01AI123010 (AW), R01AI111899 (JVG), R01AI140799 (JVG), R01MH108179 (JVG). This project was also supported by the North Carolina Policy Collaboratory at the University of North Carolina at Chapel Hill with funding from the North Carolina Coronavirus Relief Fund established and appropriated by the North Carolina General Assembly. The Microscopy Services Laboratory, Department of Pathology and Laboratory Medicine, is supported in part by P30 CA016086 Cancer Center Support Grant to the UNC Lineberger Comprehensive Cancer Center.

Author contributions AW, CEJ, WY, MK, and CD constructed LoM. AW contributed to experimental design, data interpretation, data presentation, and manuscript writing, coordinated the study, and the preparation of the manuscript. LEG performed the virus inoculations, animal necropsies, virus tittering, processing of lung tissues for RNA extraction, and contributed to the experimental design, planning, data analysis, data interpretation, and manuscript writing. CEJ performed immunofluorescence and H&E analyses, WY performed immunohistochemistry and H&E analyses, and MK performed the in-situ hybridization analysis of LoM human lung tissues. KHD, AS, SRL, and KG assisted with the *in vivo* experiments with coronavirus-infected LoMs. VJM in conjunction with KKW performed the electron microscopy analysis. GRB, AAK, MGN, and GP assisted with the EIDD-2801 experiments. FBA assisted with the pathohistological analysis. HL, HMK, TZ, POG, performed the RNA-sequencing analysis. EPB and CDJ contributed to design of RNA-sequencing experiments. RJP assisted with the immunofluorescence analysis and contributed to experimental design, data interpretation, data presentation, and manuscript writing. RSB conceived and designed experiments and contributed to data interpretation and manuscript writing. JVG conceived, designed and coordinated the study, conceived and designed experiments, and contributed to data interpretation, data presentation, and manuscript preparation.

Competing interests GP, MGN, GRB and AAK are employees of Emory and have a financial interest in molnupiravir (EIDD-2801).

Additional information

Supplementary information The online version contains supplementary material available at https://doi.org/10.1038/s41586-021-03312-w.

Correspondence and requests for materials should be addressed to J.V.G.

Peer review information *Nature* thanks the anonymous reviewers for their contribution to the peer review of this work.

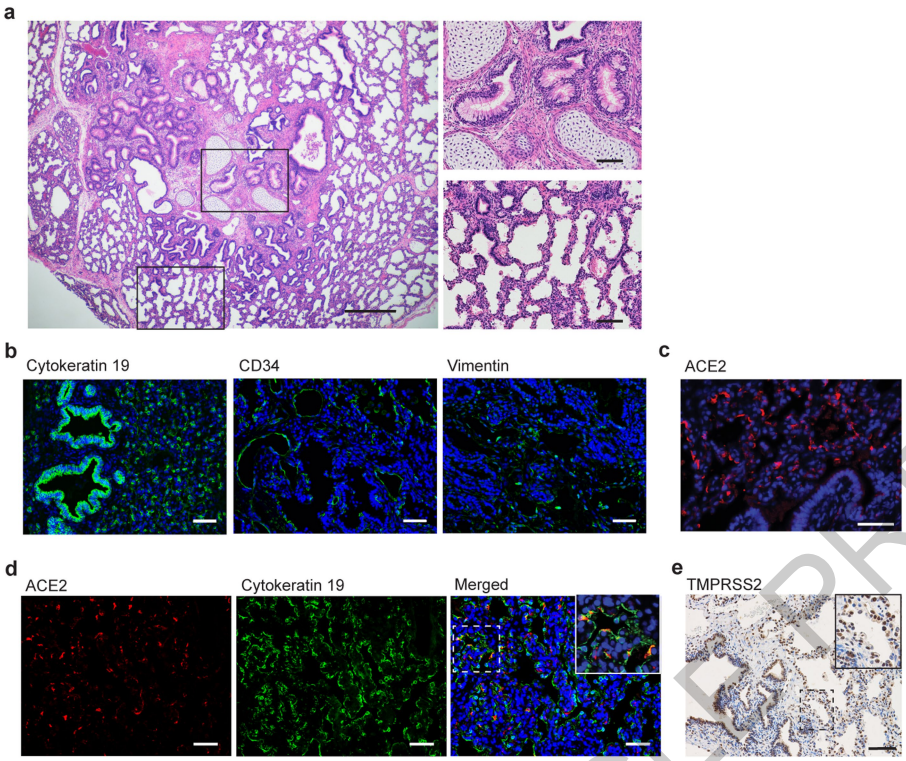

Extended Data Fig. 1 | Human epithelial cells in the human lung tissue of LoMs express ACE2. a, H&E staining of the human lung tissue of a naïve LoM (scale bars 500 um [left image] and 100 um [right images], n=6). Boxes indicate regions shown in higher magnification images (right images) of cartilaginous airways (top) and non-cartilaginous airways and alveoli (bottom). Immunofluorescence staining for **b**, human cytokeratin 19 (epithelial cells, green; nuclei, blue; scale bar 50 um), CD34 (endothelial cells, green; nuclei, blue; scale bar 50 um), and vimentin (mesenchymal cells, green; nuclei, blue; scale bar 50 um). n=8 tissues analyzed. **c**, human ACE2 in the human lung tissue of a naïve LoM (positive cells, red; nuclei, blue; scale bar 50 um, n=9). **d**, Co-staining for human ACE2 (positive cells, red) and cytokeratin 19 (positive cells, green) in naïve LoM human lung tissue (nuclei, blue; scale bar 50 um, n=9). **e**, Immunohistochemical staining for TMPRSS2 in naïve LoM human lung tissue (positive cells, brown; scale bar, 100 um; n=6). n=number of biologically independent lung tissues analyzed.

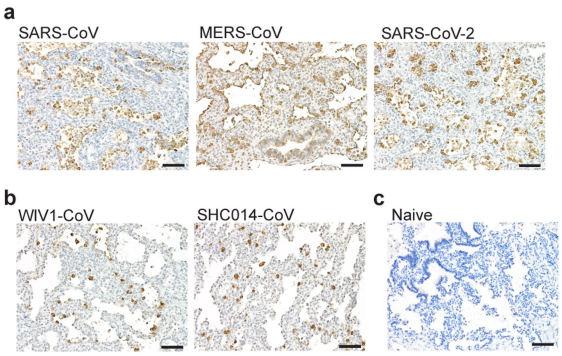

Extended Data Fig. 2 | Viral nucleoprotein in the human lung tissues of LoM infected with recently emerged human coronaviruses and bat coronaviruses. Immunohistochemical staining for virus nucleoprotein in human lung tissue collected from **a**, LoM two days post exposure to recently emerged human coronaviruses SARS-CoV (n=4), MERS-CoV (n=5), or SARS-CoV-2 (n=6), **b**, LoM two days post exposure to bat coronaviruses WIV1-CoV or SHC014-CoV (n=10), or **c**, naïve LoM (n=6). Positive cells, brown. Scale bars, 100 um. n=number of biologically independent lung tissues analyzed.

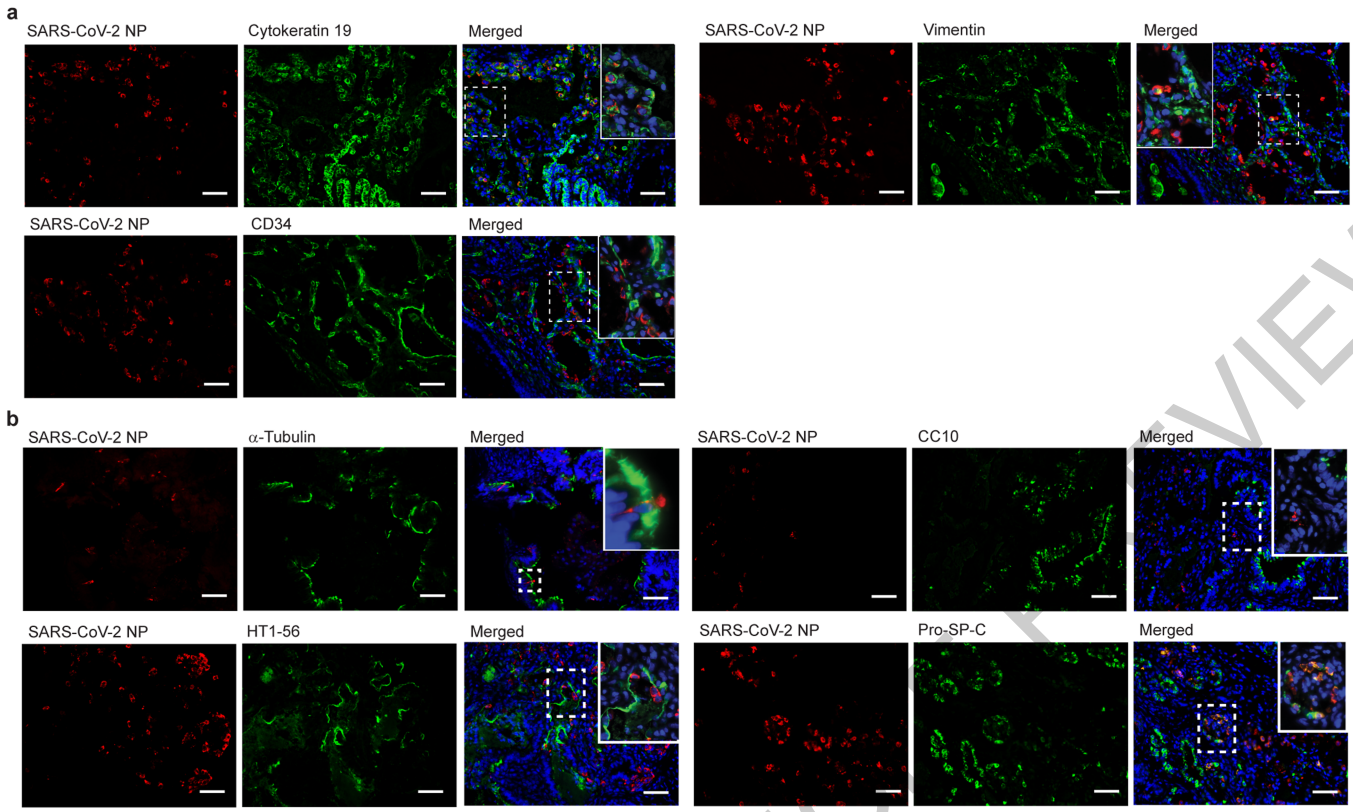

Extended Data Fig. 3 | SARS-CoV-2 infection of human epithelial cell types in the human lung tissue of LoM. Single color and merged images of those shown in Fig. 1f and g depicting co-staining of LoM human lung tissue two days following SARS-CoV-2 exposure for virus nucleoprotein (red) and **a**, and cytokeratin 19 (epithelial cells, green, n=6), CD34 (endothelial cells, green, n= 4), or vimentin (mesenchymal cells, green, n=4) or **b**, acetylated alpha-tubulin IV (ciliated cells, green, n=6), CC10 (club cells, green, n=6), HT1-56 (alveolar type 1 cells, green, n=6), or Pro-SP-C (alveolar type 2 cells, green, n=3). Nuclei, blue; scale bars 50 um. n=number of biologically independent lung tissues analyzed.

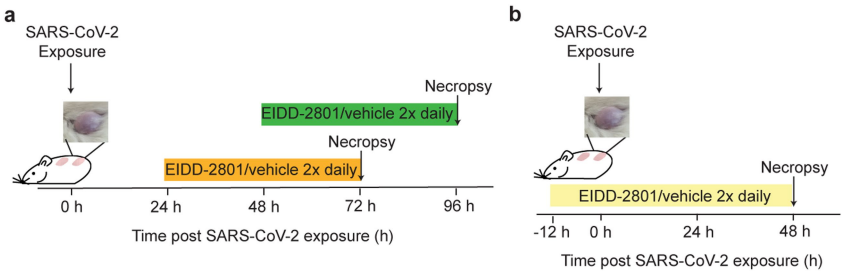

Extended Data Fig. 4 | Experimental design for the evaluation of EIDD-2801 as treatment or pre-exposure prophylaxis for SARS-CoV-2 infection. **a**, Treatment experimental design. LoM were orally administered EIDD-2801 or vehicle at 24 h or 48 h post SARS-CoV-2 exposure and every 12 h thereafter. Virus titers were measured 2 days post-treatment initiation. **b**, Pre-exposure prophylaxis experimental design. LoM were orally administered EIDD-2801 or vehicle control 12 h prior to SARS-CoV-2 exposure and every 12 h thereafter. Virus titers in human lung tissues were measured 2 days post-exposure.

Extended Data Table 1 | Description of LoM used for the analysis of human and bat coronavirus replication

Group	Mouse	Sex	Human donor	Weeks post-surgery
SARS-CoV	1	F	O32	10
	2	F	O32	10
	3	M	U32	9
	4	M	U32	9
	5	F	I33	14
	6	F	L33	10
	7	F	L33	10
	8	F	L33	10
MERS-CoV	9	M	D33	9
	10	M	D33	9
	11	M	F33	9
	12	M	F33	9
	13	F	I33	14
	14	F	L33	10
	15	F	L33	10
	16	F	L33	10
SARS-CoV-2	17	F	O32	19
	18	F	O32	19
	19	M	D33	14
	20	M	F33	14
WIV-CoV	21	M	F33	20
	22	M	F33	20
	23	M	F33	20
SHC014-CoV	24	M	F33	20
	25	M	F33	20
	26	M	F33	20

Extended Data Table 2 | Description of LoM used for the analysis of SARS-CoV-2 replication and pathogenesis over time

Group	Mouse	Sex	Human donor	Weeks post-surgery
Day 2	27	F	A31	59
	28	F	A31	59
	29	F	F32	25
	30	F	I32	19
Day 6	31	F	R30	74
	32	F	A31	59
	33	F	I32	19
	34	F	F32	25
	35	F	F32	25
Day 14	36	F	A31	59
	37	F	I32	19
	38	F	R30	74
	39	F	F32	25
	40	F	F32	25

Extended Data Table 3 | Abundance of viral transcripts detected in SARS-CoV-2 infected LoM

Group	Mouse	Sex	Human donor	Weeks post-surgery	%Viral transcripts
Day 2	1	F	A31	59	0.55301%
	41	F	I32	19	3.55979%
Day 6	31	F	R30	74	1.01818%
	32	F	A31	59	0.46368%
	33	F	I32	19	1.38159%
Day 14	37	F	I32	19	0.69389%
	39	F	F32	25	0.05856%
	42	F	A31	59	0.18557%
Naive	43	F	A31	59	N/A
	44	F	I32	19	N/A
	45	F	I32	19	N/A
	46	F	I32	19	N/A

Shown is the %viral transcripts of total transcripts sequenced from SARS-CoV-2 infected (n=8) and naïve (n=4) LoM utilized for RNA-sequencing analysis. Not applicable: N/A. Using a linear model, there was no effect of human donor on viral transcript abundance (lm() in R: estimate -0.012, p=0.103). n=number of biologically independent lung tissues analyzed.

Extended Data Table 4 | Abundance of human *ACE2* and *TMPRSS2* transcripts detected in SARS-CoV-2 infected LoM

Group	Mouse	Human donor	GAPDH (TPM)	ACE2 (TPM)	TMPRSS2 (TPM)
Day 2	1	A31	517.41	1.79	33.54
	41	I32	432.19	4.63	41.96
Day 6	31	R30	654.63	2.67	78.64
	32	A31	784.39	0.73	21.62
	33	I32	481.94	1.56	41.07
Day 14	37	I32	419.55	2.02	38.94
	39	F32	492.57	1.90	61.95
	42	A31	351.54	1.54	43.50
Naive	43	A31	2384.62	0.19	15.35
	44	I32	363.42	0.82	38.95
	45	I32	359.21	0.67	38.19
	46	I32	339.77	0.89	32.93

Shown are the abundance of human *GAPDH, ACE2,* and *TMPRSS2* transcripts sequenced in the human lung tissue collected from naïve (n=4) and SARS-CoV-2 infected (n=8) LoM. Median *ACE2* and *TMPRSS2* expression in human lung tissue of naïve mice was 0.75 TPM and 35.6 TPM respectively, which is comparable to the median expression of *ACE2* (1.01 TPM) and *TMPRSS2* (43.2 TPM) observed in human lung tissue profiled by the GTEx project (https://gtexportal.org/home/; data retrieved 10/20/2020 and 11/3/2020). No effect of human donor on *ACE2* expression (F = 2.06259641; p=0.1756 via two-sided ANOVA) was observed. Approximately the same amount of variation was observed within a human donor (mean variance within donors = 4.82) as across all donors (variance = 4.47). n=number of biologically independent lung tissues analyzed.

Extended Data Table 5 | Human interferon and cytokine genes upregulated during SARS-CoV-2 infection

		Naive	Day 2			Day 6			Day 14		
	Gene	TPM	TPM	Log2FC	p-value	TPM	Log2FC	p-value	TPM	Log2FC	p-value
Interferon genes	IFNB1	0.009721	12.89298	10.8264	N/A	0.56133	5.919101	0.000104	1.261203	6.816893	8.95E-07
	ISG15	29.11072	3529.547	7.5504869	N/A	1057.532	5.559945	N/A	680.674	4.441103	4.38E-18
	OASL	0.575651	117.7447	7.460388	N/A	24.14577	5.349643	4.82E-21	19.32386	4.837053	3.70E-40
	MX2	2.446529	207.3412	7.1723067	N/A	54.58907	4.403233	4.35E-16	73.59163	4.793127	3.89E-23
	IFITM1	75.8737	1380.718	6.8014838	N/A	841.8657	3.67271	0.027036	752.1089	3.183608	0.056391
	MX1	10.01414	1098.343	6.6205208	N/A	282.2782	4.583841	1.03E-35	320.7999	4.690323	9.58E-119
	OAS1	5.455972	427.8919	6.3944922	N/A	109.1991	4.097581	4.61E-13	128.1803	4.407948	4.03E-33
	IFIT2	5.663018	327.3042	5.8248817	N/A	40.06805	2.678602	1.04E-12	51.76333	3.021741	3.65E-11
	IFIT3	9.293879	323.3581	5.5590143	N/A	77.21678	2.973115	3.24E-09	90.51719	3.168749	9.62E-11
	OAS3	4.160792	118.0739	5.1575147	N/A	27.98228	2.619502	5.04E-13	32.44652	3.006743	1.07E-25
Cytokine genes	CXCL10	1.334587	784.985	9.4483016	N/A	51.89486	5.060381	3.36E-08	104.6776	6.211797	2.26E-28
	CXCL11	0.368657	170.7106	9.0255049	N/A	13.74948	5.100041	1.73E-13	28.97534	6.20993	4.12E-32
	CCL7	0.110614	2.114279	8.1032148	N/A	0.256785	0.939467	0.826964	4.136358	5.155454	0.0337375
	CXCL9	0.31541	20.86055	6.5863786	N/A	13.58781	5.142114	N/A	51.63909	7.324334	N/A
	CXCL8	8.329686	33.28712	6.3670255	N/A	88.08344	2.850492	N/A	6.213093	-0.60592	N/A
	CXCL2	6.093913	114.8106	5.9559545	N/A	51.26291	2.979872	0.018944	24.8723	2.026886	0.1230292
	CCL8	0.872448	31.60003	5.7008898	N/A	3.819344	2.129537	0.000334	11.39742	3.657159	2.66E-05
	CCL5	0.708453	12.48674	5.5750578	N/A	4.494502	2.620838	0.029157	19.43851	4.710446	7.17E-05
	IL6	5.42304	12.23683	5.0378314	N/A	27.2112	1.542807	N/A	3.889728	-0.96496	N/A
	IL27	0.02044	0.802539	4.5555662	N/A	0.144501	2.957134	0.168998	0.166259	2.840334	0.0473019
	CXCL3	1.665821	17.51558	4.0723405	N/A	7.100009	2.13156	0.03234	6.128888	1.776734	0.0077687
	IL17C	0.040803	0.246641	3.4322656	N/A	0.069498	1.136046	0.651685	0.079223	0.819111	0.815461
	TNF	0.252698	0.776601	2.6658632	N/A	0.370601	0.713121	0.693592	1.728727	2.737404	N/A

Transcripts per million (TPM). Log2 fold change (Log2FC) in TPM detected in LoM human lung tissues at 2 (n=2), 6 (n=3), and 14 (n=3) days post-SARS-CoV-2 exposure compared to naïve controls (n=4). P-values were calculated in DESeq2 using a two-sided Wald's test and adjusted for multiple testing using a False Discovery Rate. Not applicable (N/A): DESeq2 could not calculate a p-value due to sample size or the variance between samples. n=number of biologically independent lung tissues analyzed.

Extended Data Table 6 | Description of LoM used to evaluate the efficacy of EIDD-2801 for SARS-CoV-2 pre-exposure prophylaxis and treatment

Group	Mouse	Sex	Human donor	Weeks post-surgery
Vehicle pre-exposure prophylaxis	47	M	F33	15
	48	M	F33	15
	49	F	L33	11
	50	F	L33	11
	51	M	T33	13
	52	M	T33	13
	53	M	T33	13
	54	M	T33	13
EIDD-2801 pre-exposure prophylaxis	55	M	F33	15
	56	M	F33	15
	57	F	L33	11
	58	F	L33	11
	59	M	T33	13
	60	M	T33	13
	61	M	T33	13
	62	M	T33	13
Vehicle 24h treatment	63	F	C34	16
	64	F	C34	16
	65	F	C34	16
	66	F	C34	16
EIDD-2801 24h treatment	67	F	C34	16
	68	F	C34	16
	69	F	C34	16
	70	F	C34	16
Vehicle 48h treatment	71	F	C34	16
	72	F	C34	16
	73	F	C34	16
	74	F	C34	16
EIDD-2801 48h treatment	75	F	C34	16
	76	F	C34	16
	77	F	C34	16
	78	F	C34	16

nature research

Corresponding author(s): J. Victor Garcia

Last updated by author(s): Jan 7, 2021

Reporting Summary

Nature Research wishes to improve the reproducibility of the work that we publish. This form provides structure for consistency and transparency in reporting. For further information on Nature Research policies, see our Editorial Policies and the Editorial Policy Checklist.

Statistics

For all statistical analyses, confirm that the following items are present in the figure legend, table legend, main text, or Methods section.

n/a	Confirmed	
☐	☒	The exact sample size (*n*) for each experimental group/condition, given as a discrete number and unit of measurement
☐	☒	A statement on whether measurements were taken from distinct samples or whether the same sample was measured repeatedly
☐	☒	The statistical test(s) used AND whether they are one- or two-sided *Only common tests should be described solely by name; describe more complex techniques in the Methods section.*
☒	☐	A description of all covariates tested
☐	☒	A description of any assumptions or corrections, such as tests of normality and adjustment for multiple comparisons
☐	☒	A full description of the statistical parameters including central tendency (e.g. means) or other basic estimates (e.g. regression coefficient) AND variation (e.g. standard deviation) or associated estimates of uncertainty (e.g. confidence intervals)
☐	☒	For null hypothesis testing, the test statistic (e.g. *F*, *t*, *r*) with confidence intervals, effect sizes, degrees of freedom and *P* value noted *Give P values as exact values whenever suitable.*
☒	☐	For Bayesian analysis, information on the choice of priors and Markov chain Monte Carlo settings
☒	☐	For hierarchical and complex designs, identification of the appropriate level for tests and full reporting of outcomes
☒	☐	Estimates of effect sizes (e.g. Cohen's *d*, Pearson's *r*), indicating how they were calculated

Our web collection on statistics for biologists contains articles on many of the points above.

Software and code

Policy information about availability of computer code

Data collection	Nikon Elements BR software (version 4.30.01), Volocity software (version 6.3), Gatan Microscopy Suite software (version 3.0)
Data analysis	ImageJ/Fiji (version 2.0-rc-69/1.51w), Adobe Photoshop (version C S6), FASTQC (version 0.11.9), BBmap (version 38.86), STAR (version 2.7.5a), Salmon (version 1.2.1), DESeq2 (version 3.1.1), R (version 3.5.3 or 3.6.3), GOrilla (no version), tidyverse (version 1.3.0), PCATools (version 1.2.0), Sqldf (version 0.4-11), na.tools (version 0.3.1), ggbiplot (version 0.55), ggplot2 (version 3.3.1), dplyr (version 0.8.4), Graphpad Prism (version 8.0.0)

For manuscripts utilizing custom algorithms or software that are central to the research but not yet described in published literature, software must be made available to editors and reviewers. We strongly encourage code deposition in a community repository (e.g. GitHub). See the Nature Research guidelines for submitting code & software for further information.

Data

Policy information about availability of data

All manuscripts must include a data availability statement. This statement should provide the following information, where applicable:

- Accession codes, unique identifiers, or web links for publicly available datasets
- A list of figures that have associated raw data
- A description of any restrictions on data availability

Gene-expression data are available at the Gene Expression Omnibus (GEO) repository (accession: GSE155286). Source data is provided for Fig. 1b,c and Fig. 4a-d. All other data is available from corresponding authors on reasonable request. Publicly available data sets used in this study: 1) sequence of the SARS-CoV-2 strain 2019-nCoV/USA-WA1/2020 (GenBank accession: MN985325.1) and 2) human lung tissue gene expression data profiled by the GTEx project (https://gtexportal.org/home/; data retrieved 10/20/2020 and 11/3/2020).

Field-specific reporting

Please select the one below that is the best fit for your research. If you are not sure, read the appropriate sections before making your selection.

☒ Life sciences ☐ Behavioural & social sciences ☐ Ecological, evolutionary & environmental sciences

For a reference copy of the document with all sections, see nature.com/documents/nr-reporting-summary-flat.pdf

Life sciences study design

All studies must disclose on these points even when the disclosure is negative.

Sample size	No statistical methods were used to predetermine sample size. To aid statistical analysis, at least 3 samples were used for each group, unless otherwise noted. At least three animals were utilized for each virus and time point. The number of animals per group was also influenced by the number different analyses performed for each experiment (e.g. virus titer, immunofluorescence/immunohistochemistry, electron microscopy, and/or RNA-sequencing) and so that at least three animals per group were represented for each downstream analysis unless otherwise noted.
Data exclusions	No data was excluded from analysis.
Replication	For the analysis of coronavirus replication in LoM, SARS-CoV and MERS-CoV infections represented 4 human donor cohorts. For the analysis of SARS-CoV-2 replication over time, 4 human donor cohorts were represented. For the analysis of the protective efficacy of EIDD-2801, 3 human donor cohorts were represented and the experiment performed twice. All attempts at replication were successful.
Randomization	No randomization was used to determine how samples/animals were allocated to experimental groups or processed. Mice were allocated to groups based on their implant sizes and their donor cohort to keep experimental groups relatively equivalent with these covariates. Whole implants or pieces of implants (depending on size) from each animal were allocated for analysis by virus titer, immunofluorescence/ immunohistochemistry, electron microscopy, and/or RNA-sequencing so that at least three animals per group were represented (with the exception of the day 2 RNA-seq analysis) and human donor cohorts were represented as equivalently.
Blinding	The investigators were not blinded to group allocation for data collection and analysis. For virus titer measurements, the infecting strain determines what type of cells are used for plaque assays. For example, MERS-CoV is titered on Vero CCL81 cells while SARS-CoV, SARS-CoV-2, WIV-1, and SHC014 are titered using Vero E6 cells. For the RNA-seq analysis, viral and human gene transcripts were analyzed from the same sample. For RNAscope, immunoflourescense, and immunohistochemistry the infecting strain also determines which RNA probe or antibody is used to analyze tissues sections for detection of virus infected cells. H/E staining was often done in parallel. Due to COVID-19 restrictions, personnel who performed histological assays also performed data analysis. For electron microscopy analysis, only SARS-CoV-2 infected human lung tissues were analyzed. Personnel at the UNC Animal Histopathology and Clinical Chemistry Core who performed MSB staining were not privy to group allocations.

Reporting for specific materials, systems and methods

We require information from authors about some types of materials, experimental systems and methods used in many studies. Here, indicate whether each material, system or method listed is relevant to your study. If you are not sure if a list item applies to your research, read the appropriate section before selecting a response.

Materials & experimental systems

n/a	Involved in the study
☐	☒ Antibodies
☐	☒ Eukaryotic cell lines
☒	☐ Palaeontology and archaeology
☐	☒ Animals and other organisms
☒	☐ Human research participants
☒	☐ Clinical data
☒	☐ Dual use research of concern

Methods

n/a	Involved in the study
☒	☐ ChIP-seq
☒	☐ Flow cytometry
☒	☐ MRI-based neuroimaging

Antibodies

Antibodies used	anti-ACE2; clone: Polyclonal IgG; dilution 1:200 dilution; supplier: R&D systems; catalog: AF933 ; lot: HOK0320032; application: IF; https://www.rndsystems.com/products/human-hamster-ace-2-antibody_af933 anti-Acetylated alpha-tubulin; clone: 6-11B-1; dilution: 1:500; supplier: Zymed; catalog: 32-2700; lot: 60806682R; application: IF; https://www.thermofisher.com/antibody/product/Acetyl-alpha-Tubulin-Lys40-Antibody-clone-6-11B-1-Monoclonal/32-2700 anti-CC10; clone: E-11; dilution: 1:500; supplier: Santa Cruz Biotech; catalog: SC-365992; lots: B2219, K10106; application: IF; https://www.scbt.com/p/cc10-antibody-e-11?requestFrom=search

anti-CD34; clone: QBEnd10; dilution: 1:100; supplier: Dako; catalog: M7165; lot: 20011397; application: IF; https://www.agilent.com/store/productDetail.jsp?catalogId=M716501-2

anti-Cytokeratin19; clone: A53-B/A2; dilution: 1:250; supplier: Abcam; catalog: ab7754; lot: GR3226692-4; application: IF; https://www.abcam.com/cytokeratin-19-antibody-a53-ba2-cytoskeleton-marker-ab7754.html

anti-HT1-56; dilution: 1:150; supplier: Terrace Biotech; catalog: TB-29; lot: AHT1-56 HM29; application: IF; https://www.terracebiotech.com/antibodies

anti-MERS nucleocapsid; clone: Polyclonal; dilution: 1:2,000; supplier: LS Bio; catalog: LS-C483529; lot: 127989; application: IHC; https://www.lsbio.com/antibodies/mers-cov-nucleoprotein-antibody-elisa-wb-western-ls-c483529/496447

anti-Pro-SP-C; clone: Polyclonal; dilution: 1:500; supplier: Seven Hills; catalog: WRAB9337; lots: 458, 0206A; application: IF; https://www.sevenhillsbioreagents.com/products/anti-pro-sp-c-rabbit-n-terminal?_pos=1&_sid=51b111a78&_ss=r

anti-SARS nucleocapsid; clone: Polyclonal IgG; dilution: 1:500; supplier: Invitrogen; catalog: PA1-41098, lot: VC2962205; application: IF and IHC; https://www.thermofisher.com/antibody/product/SARS-Coronavirus-Nucleocapsid-Antibody-Polyclonal/PA1-41098

anti-SARS nucleocapsid; dilution: 1:1,000; supplier: Baric Laboratory; application: IF

anti-TMPRSS2; clone: Polyclonal Ig; dilution: 1:100; supplier: MyBioSource; catalog: MBS9215011, lot:SH200730AC; application: IHC; https://www.mybiosource.com/polyclonal-human-antibody/tmprss2/9215011

anti-Vimentin; clone: V9; dilution: 1:100; supplier: Abcam; catalog: ab8069; lot: GR3226692-4; application: IF; https://www.abcam.com/vimentin-antibody-v9-cytoskeleton-marker-ab8069.html

anti-Mouse IgG heavy and light chains-AlexaFluor 488; clone: donkey polyclonal IgG; dilution: 1:1,000; supplier: Invitrogen; catalog: A21202; lot: 2147618; application: IF; https://www.thermofisher.com/antibody/product/Donkey-anti-Mouse-IgG-H-L-Highly-Cross-Adsorbed-Secondary-Antibody-Polyclonal/A-21202

anti-Rabbit IgG heavy and light chains-AlexaFluor 488; clone: donkey polyclonal IgG; dilution: 1:1,000; supplier: Invitrogen; catalog: A21206; lot: 2156521; application: IF; https://www.thermofisher.com/antibody/product/Donkey-anti-Rabbit-IgG-H-L-Highly-Cross-Adsorbed-Secondary-Antibody-Polyclonal/A-21206

anti-Goat IgG heavy and light chains-AlexaFluor 594; clone: donkey Polyclonal IgG; dilution: 1:1,000; supplier: Invitrogen; catalog: A11058; supplier: 2045324; application: IF; https://www.thermofisher.com/antibody/product/Donkey-anti-Goat-IgG-H-L-Cross-Adsorbed-Secondary-Antibody-Polyclonal/A-11058

anti-Mouse IgG heavy and light chains-AlexaFluor Plus 594; clone: donkey Polyclonal IgG; dilution: 1:1,000; supplier: Invitrogen A32744; catalog: UL292347; application: IF; https://www.thermofisher.com/antibody/product/Donkey-anti-Mouse-IgG-H-L-Highly-Cross-Adsorbed-Secondary-Antibody-Polyclonal/A32744

anti-Rabbit IgG heavy and light chains-AlexaFluor Plus 594; clone: donkey Polyclonal IgG; dilution: 1:1,000; supplier: Invitrogen A32754; catalog: VB292347; application: IF; https://www.thermofisher.com/antibody/product/Donkey-anti-Rabbit-IgG-H-L-Highly-Cross-Adsorbed-Secondary-Antibody-Polyclonal/A32754

anti-Mouse IgG heavy and light chains-AlexaFluor 647; clone donkey Polyclonal IgG; dilution: 1:1,000; supplier: Invitrogen; catalog: A31571; lot: 2045337; application: IF; https://www.thermofisher.com/antibody/product/Donkey-anti-Mouse-IgG-H-L-Highly-Cross-Adsorbed-Secondary-Antibody-Polyclonal/A-31571

Validation

The specificity of the antibodies purchased from commercial sources (R&D Systems, Zymed, Santa Cruz Biotech, Dako, Abcam, Terrace Biotech, LS Bio, Seven Hills, and Invitrogen) were validated by the manufacturer as noted on their website (links provided above for each antibody). anti-SARS nucleoprotein mouse serum was produced by the Baric laboratory and validated for immunohistochemistry and immunofluorescence using COVID-19 autopsy lung sections and SARS-CoV-2 infected human airway epithelial cell cultures (https://www.cell.com/cell/pdf/S0092-8674%2820%2930675-9.pdf).

Eukaryotic cell lines

Policy information about cell lines

Cell line source(s)	Vero E6 cells and Vero CCL81 cells were purchased from ATCC
Authentication	Cell lines were authenticated by morphological identification and virus susceptibility profiles.
Mycoplasma contamination	Cell lines were tested negative for mycoplasma by the supplier.
Commonly misidentified lines (See ICLAC register)	No commonly misidentified cell lines were used

Animals and other organisms

Policy information about studies involving animals; ARRIVE guidelines recommended for reporting animal research

Laboratory animals	Lung-only mice (LoM) were constructed using 12-21 week old male and female NOD.Cg-Prkdcscid Il2rgtm1Wjl/SzJ mice (NSG; The Jackson Laboratory, Bar Harbor, ME) mice. Mice were housed in a temperature (20-23°C) and humidity (30-70%) controlled room on a 12 hour light/12 hour dark schedule.
Wild animals	The study did not involve wild animals.
Field-collected samples	The study did not involve field collected samples.
Ethics oversight	Animal studies were carried out according to protocols approved by the Institutional Use and Care Committee at UNC-Chapel Hill and in adherence to the NIH Guide for the Care and Use of Laboratory Animals.

Note that full information on the approval of the study protocol must also be provided in the manuscript.